Global Biogeochemical Cycles

RESEARCH ARTICLE
10.1029/2025GB008936

A Revised Estimate of Calcium Carbonate Dissolution in Coastal and Shelf Sediments Suggests Large Shelf Exports in the Marine $CaCO_3$ Cycle

Cedric Goossens[1], Sebastiaan J. van de Velde[2,3], and Filip J. R. Meysman[1]

[1]Department of Biology, University of Antwerp, Antwerp, Belgium, [2]Department of Marine Science, Ōtākou Whakaihu Waka University of Otago, Dunedin, New Zealand, [3]Earth Sciences New Zealand, Wellington, New Zealand

Key Points:

- Carbonate-poor shelf dissolution (5 ± 9 Tmol per year) might be comparable to dissolution in coral reefs and lagoons (5 ± 1 Tmol per year)
- An important fraction of the shelf carbonate is likely transported from the coastal zone to the deep sea via cross-shelf export
- An apparent missing source of ~11 Tmol per year in the global carbonate budget (shelf + deep ocean) likely results from rate uncertainties

Supporting Information:

Supporting Information may be found in the online version of this article.

Correspondence to:

C. Goossens,
Cedric.Goossens@uantwerpen.be

Citation:

Goossens, C., van de Velde, S. J., & Meysman, F. J. R. (2026). A revised estimate of calcium carbonate dissolution in coastal and shelf sediments suggests large shelf exports in the marine $CaCO_3$ cycle. *Global Biogeochemical Cycles*, *40*, e2025GB008936. https://doi.org/10.1029/2025GB008936

Received 15 OCT 2025
Accepted 9 MAR 2026

Abstract Calcium carbonate ($CaCO_3$) dissolution plays a key role in the marine carbon and alkalinity cycles and the regulation of atmospheric CO_2 levels across geological time scales. Until now, most attention has focused on dissolution in the deep sea, while dissolution in coastal and shelf environments remains poorly constrained. Here, we present a synthesis of $CaCO_3$ dissolution rates in sediments of coastal and shelf environments and integrate them into an updated global marine $CaCO_3$ budget. The highest areal dissolution rates occur in coral reefs and lagoons, and in seagrass-dominated banks and bays, as these sediments combine high amounts of soluble high-magnesium calcite with deep oxygen penetration and high organic matter input that facilitate dissolution. Nevertheless, carbonate-poor shelves contribute as much (~45%) as coral reefs and lagoons to global coastal and shelf carbonate dissolution. Total coastal and shelf dissolution is estimated at 11 ± 9 Tmol yr^{-1} and thus provides ~8% of the total $CaCO_3$ dissolution in the ocean. Combining these dissolution rates with published estimates of production, terrestrial input, and burial, mass balance closure requires an off-shelf lateral export of ~15 Tmol $CaCO_3$ yr^{-1}. Although this estimate carries large uncertainty (>100%), it suggests that a significant fraction of the $CaCO_3$ produced on the shelf is transferred from a short-term climate buffer in the shelf seafloor to a long-term climate buffer in the deep-sea seafloor.

Plain Language Summary Calcium carbonate is an abundant mineral in the ocean and is formed by corals and shell-forming organisms. While calcium carbonate formation releases CO_2 from the ocean to the atmosphere, its dissolution captures CO_2. The balance between formation and dissolution influences the ocean's alkalinity cycle and hence regulates the climate via atmospheric CO_2 buffering. While most studies have focused on dissolution in the deep ocean, we show that shallow coastal and continental shelf areas also play an important role. We combined published data to estimate how much calcium carbonate dissolves in coastal and shelf environments. Our results show that carbonate dissolution in shallow environments represents a considerable fraction of the carbonate dissolution in the global ocean. We also suggest that a fraction of the shelf calcium carbonate is carried off the shelf toward the deep sea, where it becomes part of the long-term carbonate cycle.

1. Introduction

In recent years, the ocean has received growing attention in the context of carbon dioxide removal (CDR) owing to its large CO_2 storage potential (Friedlingstein et al., 2025; Oschlies et al., 2023). One of the proposed CDR methods is ocean alkalinity enhancement (OAE), which targets a deliberate addition of alkalinity (A_T) levels to surface waters, thereby increasing the oceanic uptake of atmospheric CO_2 (Oschlies et al., 2023; Renforth & Henderson, 2017). This recent attention for OAE has also revived an interest in the A_T budget of the ocean, as OAE applications could modulate the various natural processes that produce and consume A_T (Bach, 2024; van de Velde et al., 2026). One key part of the ocean alkalinity budget is the internal cycling of calcium carbonate ($CaCO_3$), which is formed by planktonic or benthic calcifying organisms in surface waters, and dissolves again in either the water column or the sediment (Middelburg et al., 2020; Milliman & Droxler, 1996; Zeebe & Wolf-Gladrow, 2001). The precipitation of 1 mol of $CaCO_3$ consumes 2 mol of A_T, whereas dissolution produces 2 mol of A_T per 1 mol of $CaCO_3$.

$$Ca^{2+} + 2HCO_3^- \leftrightarrow CaCO_3 + CO_2 + H_2O \quad (1)$$

Calcium carbonate occurs in the polymorphic forms aragonite and calcite, and calcite can be further classified as low- or high-magnesium calcite, depending on how much $MgCO_3$ is incorporated in its structure (Haese et al., 2014). A key factor determining precipitation or dissolution is the $CaCO_3$ saturation state of seawater, which primarily depends on the concentration of CO_3^{2-}, as the concentration of Ca^{2+} in seawater is high and hence less variable across space and time (Zeebe & Wolf-Gladrow, 2001). Surface waters are generally oversaturated with respect to the $CaCO_3$ mineral forms and thus precipitation is thermodynamically favored over dissolution (Kleypas, 2011; Morse & Mackenzie, 1990). In deeper waters, however, the solubility of $CaCO_3$ increases due to an increase in pressure and a decrease in temperature (Millero, 2007). Additionally, aerobic mineralization of organic matter produces CO_2, which reduces the pH and carbonate ion concentration in seawater (Boudreau et al., 2018). Therefore, when $CaCO_3$ minerals descend into deeper waters, the saturation state decreases to unity at a given water depth, called the (aragonite or calcite) saturation horizon. Below this horizon, seawater becomes undersaturated, and $CaCO_3$ minerals start to dissolve in the water column and sediment (Ridgwell & Zeebe, 2005). The dynamic balance between carbonate precipitation and dissolution in oceans and sediments forms a natural negative feedback mechanism, termed "carbonate compensation," which regulates atmospheric CO_2 levels on millennial timescales (Archer, 1996; Sarmiento & Gruber, 2006).

Above the saturation horizon, undersaturation can occur in specific environments, such as degrading particle aggregates in the water column or the pore water of sediments. These environments typically have limited exchange with their surrounding waters, allowing the CO_2 from aerobic mineralization to build up until undersaturation is achieved and $CaCO_3$ minerals start to dissolve (Dean et al., 2024; Morse & Mackenzie, 1990; Subhas et al., 2022; Sulpis et al., 2021). This process is referred to as metabolic carbonate dissolution:

$$CaCO_3 + CH_2O + O_2 \rightarrow Ca^{2+} + 2HCO_3^- \quad (2)$$

Although coastal and shelf sediments are positioned far above the saturation horizon, recent studies have shown that $CaCO_3$ dissolution in shallow marine sediments increases with decreasing saturation state (Eyre et al., 2018; Lunstrum & Berelson, 2022). Coastal and shelf sediments are also subject to high rates of advection, either via advective flow induced by currents (Huettel & Rusch, 2000; Riedl et al., 1972; Webb & Theodor, 1968) or by bioirrigation induced by benthic fauna (Aller & Yingst, 1985; Gust & Harrison, 1981; Huettel & Gust, 1992). Consequently, any changes in the water column are rapidly transferred to the pore waters on a timescale of days to years. Coastal and shelf environments are shallow and generally have well-mixed water columns, and so, they equilibrate far more rapidly with the atmosphere than deep-sea sediments. Hence, coastal and shelf sedimentary $CaCO_3$ dissolution may respond more rapidly to ocean acidification and changes in saturation state and could help buffer atmospheric CO_2 change on a timescale of years to decades (i.e., relevant to the current climate challenge; Eyre et al., 2014; van de Velde et al., 2026).

In global carbonate budgets, however, $CaCO_3$ dissolution is often calculated as the difference between production and accumulation/burial, rather than directly from observational dissolution data (Iglesias-Rodriguez et al., 2002; Milliman, 1993; Milliman & Droxler, 1996; Schneider & Schulz, 2016; Smith & Mackenzie, 2016; Wollast, 1994). This approach induces substantial uncertainties in coastal and shelf seafloor $CaCO_3$ dissolution rates and potentially obscures any lateral carbonate transport (i.e., terrestrial carbonate input or off-shelf carbonate transport). In this study, we compiled the available seafloor $CaCO_3$ dissolution data from coastal and shelf sediments. We discuss the drivers of sedimentary $CaCO_3$ dissolution and present an updated budget of the coastal and shelf $CaCO_3$ cycles.

2. Methods

2.1. Data Collection

$CaCO_3$ dissolution rates (R_{diss}) were taken from studies in which they were either directly reported or derivable from supplementary data (see Figure 1 for data locations). These reported dissolution rates were originally obtained through different methods (Table S1 in Supporting Information S1): (a) reaction-transport modeling based on pore-water profiles of A_T, calcium (Ca^{2+}), oxygen (O_2), and dissolved inorganic carbon (DIC); (b) the alkalinity anomaly technique (Smith & Key, 1975), which measures A_T in the overlying water; (c) measurements of A_T, Ca^{2+}, and δ^{13}C-DIC fluxes in both in situ and ex situ incubations; and (d) direct mass loss measurement from carbonate substrates implanted in natural sediments. Values of R_{diss} were compared to carbon-based mineralization rates (R_{min}), which were either directly reported or were reported as oxygen fluxes, which we

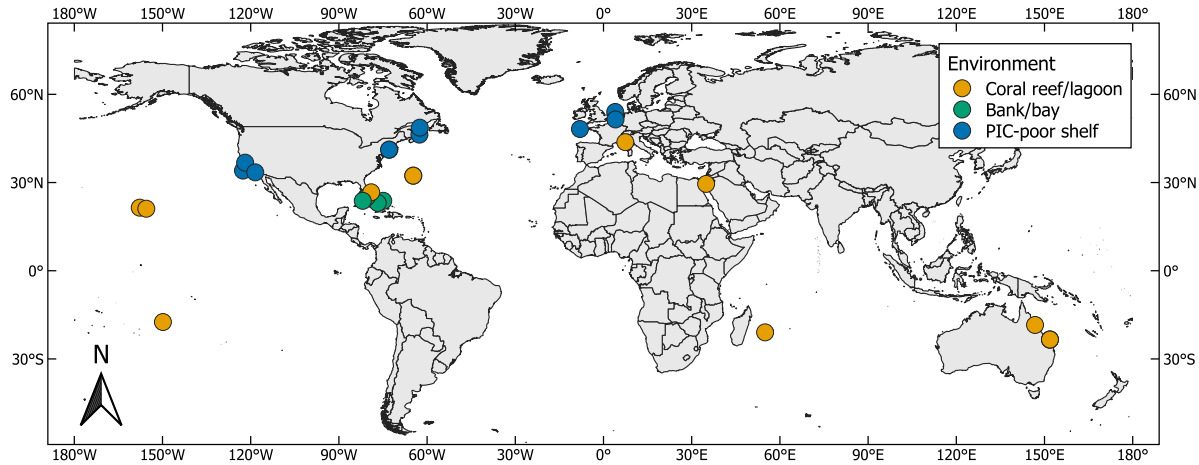

Figure 1. Map indicating the locations for which data were used in this study, categorized according to the type of environment (see Table S2 in Supporting Information S1 for coordinates). PIC-poor shelf indicates carbonate-poor shelf. Data points were slightly offset to improve visibility.

transformed into R_{min} values using a respiratory DIC:O_2 quotient of 0.9 for inner shelf sediments (Jørgensen et al., 2022). To avoid the confounding effects of photosynthesis and calcification, data were only retained for dark conditions (i.e., dark incubations and/or night-time in situ measurements). Data points from water depths greater than 500 m were excluded from the analysis as this is considered beyond the maximum water depth of the global shelf (Durán & Guillén, 2018; Harris & Macmillan-Lawler, 2016).

Study sites were classified according to Milliman (1993) into four types of coastal and shelf environments based on their carbonate production and accumulation rates (see Table 1): (a) coral reefs and lagoons, (b) banks and bays, (c) carbonate-rich shelves (>70 wt.% $CaCO_3$), and (d) carbonate-poor shelves (<70 wt.% $CaCO_3$; see Milliman, 1993; Milliman & Droxler, 1996 for a more detailed description of the classification). While reefs and lagoons comprise a mosaic of benthic habitats, ranging from live reef frameworks to sediment-dominated areas, they are grouped together here because several of the included studies infer carbonate dissolution from alkalinity changes in the overlying water column. These measurements integrate fluxes over larger benthic surfaces and therefore represent averaged signals despite small-scale habitat heterogeneity. Banks and bays were classified into vegetated and non-vegetated systems (the former having higher local primary production and organic input than the latter). Among the three major vegetated coastal ecosystems (seagrass meadows, mangrove forests, and salt marshes), data on carbonate dissolution were almost only available for (sub)tropical seagrass ecosystems. As such, banks and bays were further subdivided based on the presence or absence of seagrasses. Carbonate-rich shelves are found in extratropical or cold-water environments (see Smith & Mackenzie, 2016 for an extensive list), but no studies were found that reported dissolution rates. Carbonate-poor shelves were further subdivided into permeable sands (≥63 μm grain size) and cohesive muds (silts and muds; <63 μm) according to the Wentworth classification scale. Finally, it should be noted that $CaCO_3$ dissolution data from studies within each type of coastal and shelf environment were pooled without taking additional environmental (e.g., temperature,

Table 1
Classification of Coastal and Shelf Environments and Associated $CaCO_3$ Production Rates

Environment	Area[a] (10^{12} m^2)	$CaCO_3$ production[a] (mol m^{-2} yr^{-1})	$CaCO_3$ mineral phases[b,c,d,e]
Coral reef/lagoon	0.90	18	Aragonite, HMC, LMC
Bank/bay	0.40	5	Aragonite, HMC, LMC
Carbonate-rich shelf	1.3	3	Aragonite, LMC
Carbonate-poor shelf	19.4	1	Aragonite, LMC

Note. Production rates represent global averages. The corresponding mineral phases formed in each environment are listed (HMC, high-magnesium calcite; LMC, low-magnesium calcite). [a]Smith and Mackenzie (2016). [b]Andersson et al. (2008). [c]Chave (1954). [d]Chave (1962). [e]Morse and Mackenzie (1990).

depth) or temporal (e.g., seasonal or annual variability) factors into account. While such factors affect dissolution rates in the short term, our aim was to arrive at a long-term average dissolution rate to improve the $CaCO_3$ budget, which warrants the pooling of studies.

2.2. Statistical Data Analysis

A meta-analysis was conducted to estimate mean dissolution rates and 95% confidence intervals per coastal and shelf environment based on the dissolution rates and variances reported in the individual studies (Table S3 in Supporting Information S1). Variances that were not directly reported in individual studies were either calculated or estimated from the reported data points. Mean dissolution rates per study were calculated using dissolution rates from within-study clusters (i.e., sampling stations or sampling events) considering the variance per cluster (i.e., sampling replicates):

$$\sigma^2 = \frac{\sigma_b^2}{m} + \frac{\sigma_w^2}{n}$$

In this formula, σ_b^2 represents the between-variance for m sample clusters, which was estimated as the variance of cluster means around the overall mean (s_b^2), whereas σ_w^2 represents the within-variance for n sampling replicates per cluster, which is estimated as follows (here shown for two clusters, for which n is the number of replicates and s_w^2 is the within-variance per cluster):

$$\sigma_w^2 = \frac{s_{w1}^2(n_1 - 1) + s_{w2}^2(n_2 - 1)}{n_1 + n_2 - 2}$$

When insufficient information was available to calculate the total variance, a conservative estimate was given by calculating the upper boundary of the 95% confidence interval of the highest observed variance in that coastal or shelf environment (for which $n \geq 5$ to remove studies with limited data):

$$\sigma^2 = \frac{(n-1)\,s^2}{\chi^2_{(\alpha=0.025)(n-1)}}$$

The term s^2 represents the highest observed sample variance, and the population is assumed to follow a chi-square distribution following Cochran's theorem.

To estimate mean dissolution rates per coastal and shelf environment, a random-effects model was developed using the CRAN:metafor package (Viechtbauer, 2010) in R. This model incorporates both within-study and between-study variability and assumes that the effect may vary across studies due to environmental and methodological variability. To estimate the between-study variance, the Restricted Maximum Likelihood method was used in combination with the Hartung-Knapp adjustment to account for expected heterogeneity and small sample sizes. Heterogeneity was then assessed using three statistical metrics to evaluate the appropriateness of the random-effects model for the analysis: Q quantifies total variability among study estimates (calculated as the weighted sum of squared deviations from the pooled dissolution rate) and is compared to a chi-square distribution; τ^2 estimates absolute between-study variance and is compared to the pooled dissolution rate; and I^2 indicates the proportion of total variance attributed to heterogeneity rather than within-study variance (Borenstein et al., 2009). While there is no strictly defined threshold, the following categorization has been suggested (Higgins, 2003): $I^2 = 25\%$ is considered low, $I^2 = 50\%$ moderate, and $I^2 = 75\%$ high. Subgroups for banks and bays were included to account for seagrass presence due to its significant impact on dissolution rates, as discussed in the following section. Mud and sand subgroups for carbonate-poor shelves were also included. Dissolution rates for each environment were obtained from the model and then integrated over their global areas (Table 1).

2.3. Coastal and Shelf $CaCO_3$ Budget

Integrated $CaCO_3$ dissolution rates were combined with production, burial, and additional input rates from literature to create a $CaCO_3$ budget for the global coastal and shelf environment. The residual required to balance the budget was calculated as

$$\text{Residual} = \text{production} + \text{additional input} - \text{burial} - \text{dissolution}$$

Since rate uncertainties from literature were not always provided or comparable, they were reported in this study as either G (good; around 50% uncertainty), F (fair; around 100% uncertainty), or P (poor; >100% uncertainty), following the convention adopted in previous $CaCO_3$ budget estimates (Iglesias-Rodriguez et al., 2002; Milliman & Droxler, 1996). Unknown uncertainties were given a question mark (?).

2.3.1. $CaCO_3$ Production

Carbonate production in coastal and shelf sediments consists of planktonic and benthic production, with the latter being the predominant source (Milliman & Droxler, 1996; Smith & Mackenzie, 2016). Planktonic coastal and shelf production is poorly constrained, as most calcification rate measurements have been performed in the open ocean (Balch et al., 2007; Berelson et al., 2007). In this study, we adopted the crude estimate of Milliman and Droxler (1996) of 20 g $CaCO_3$ m^{-2} yr^{-1}, resulting in a total of 4.4 Tmol yr^{-1} for the coastal and shelf environments (0.2, 0.1, 0.2 and 4 Tmol yr^{-1} for coral reefs and lagoons, banks and bays, carbonate-rich and carbonate-poor shelves, respectively) with an attributed uncertainty of >100% (P) due to a lack of more detailed studies.

For benthic production of coral reefs and lagoons, the global area (0.90×10^{12} m^2; Table 1) was subdivided into 2 levels. At the first level, reefs and lagoons were categorized as either visible (0.15×10^{12} m^2) or submerged (0.75×10^{12} m^2), following Smith and Mackenzie (2016). At the second level, visible and submerged areas were categorized as live reefs (20%) or lagoon (80%; Milliman, 1993). Carbonate production rates derived from literature were 50 ± 30 mol m^{-2} yr^{-1} for visible live reefs (standard deviation based on 28 studies; Falter et al., 2013), 10 mol m^{-2} yr^{-1} for submerged live reefs (middle value of reported range of 1–20 mol m^{-2} yr^{-1}; Vecsei, 2004), and 8 ± 4 mol m^{-2} yr^{-1} for visible and submerged lagoons (standard deviation based on 5 studies; Smith & Kinsey, 1976). The combined benthic and planktonic production rate for coral reefs and lagoons was then estimated at 9 Tmol yr^{-1}, with an uncertainty of 50% (G).

For banks and bays, Milliman (1993) and Milliman and Droxler (1996) summarized benthic production rates from the literature, ranging from 3 to 5 mol m^{-2} yr^{-1}. An estimated rate of 5 mol m^{-2} yr^{-1} with an uncertainty of 100% was reported, which we adopted in this study, resulting in a combined benthic and planktonic bank and bay production rate of 2 Tmol yr^{-1} with an uncertainty of 100% (F).

The carbonate-rich shelf benthic production rate was adopted from Smith and Mackenzie (2016), who reported a mean of 5.3 ± 5.3 mol m^{-2} yr^{-1} (standard deviation based on 24 studies). Given the spread of the data, however, they used the median value of 3 mol m^{-2} yr^{-1}, which was also used in this study, resulting in a combined benthic and planktonic carbonate-rich shelf production rate of 4 Tmol yr^{-1}, with an estimated uncertainty of 100% (F).

The carbonate-poor shelf benthic production rate was based on a global assessment of echinoderm calcification, a major contributor to carbonate production in non-reef sedimentary shelf environments (Lebrato et al., 2010). A mean production rate of 0.8 mol m^{-2} yr^{-1} was reported, which stemmed from a very wide range of values ($1.17 \times 10^{-8} - 15.1$ mol m^{-2} yr^{-1}, based on 164 studies). We adopted the mean value and included an upward adjustment, following Smith and Mackenzie (2016), to account for the contribution of other calcifying organisms in addition to echinoderms. A benthic production rate of 1 mol m^{-2} yr^{-1} was used in this study, resulting in a combined benthic and planktonic carbonate-poor shelf production rate of 23 Tmol yr^{-1}, with an estimated uncertainty of >100% (P).

2.3.2. $CaCO_3$ Burial

Burial rates and uncertainties were derived from reported fractions and uncertainties of total $CaCO_3$ production that are eventually buried (80% for coral reefs and lagoons, 50% for banks and bays, 50% for carbonate-rich shelves and 25% for carbonate-poor shelves; Milliman, 1993; Milliman & Droxler, 1996). This resulted in global burial rates of 7 Tmol yr^{-1} for coral reefs and lagoons (uncertainty of 50%; G), 1 Tmol yr^{-1} for banks and bays (uncertainty of 100%; F), 2 Tmol yr^{-1} for carbonate-rich shelves (uncertainty of >100%; P) and 6 Tmol yr^{-1} for carbonate-poor shelves (uncertainty of 50%; G).

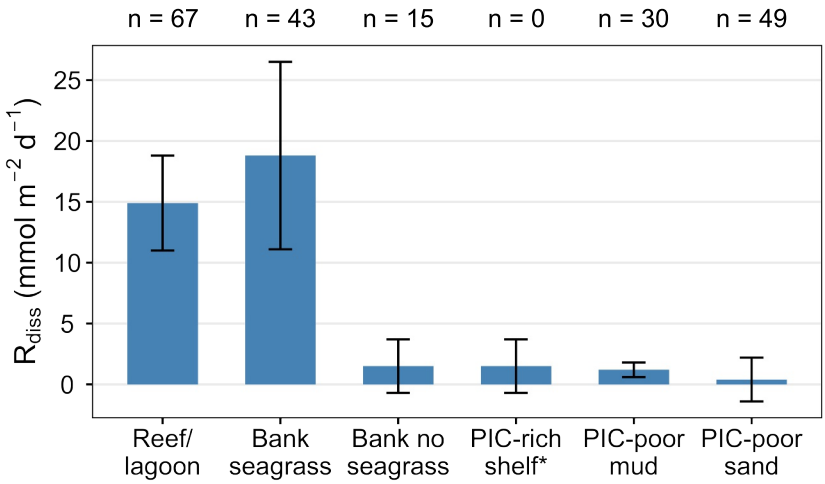

Figure 2. Mean dissolution rates (R_{diss}) estimated by the random-effects model for different coastal and shelf environments (n = number of data points per category; error bars indicate 95% confidence intervals). PIC-rich shelf: carbonate-rich shelf sediment, PIC-poor mud: carbonate-poor muddy shelf sediment, PIC-poor sand: carbonate-poor sandy shelf sediment. *The rate of banks without seagrass was used as a proxy for carbonate-rich shelf, since no data was available (see text).

2.3.3. Additional $CaCO_3$ Input

Additional $CaCO_3$ input comes from rivers across the globe (3.1 ± 0.3 Tmol yr^{-1}) and meltwater discharge and ice-rafted debris from Greenland and Antarctica (0.8 ± 0.3 Tmol yr^{-1}; Müller et al., 2022), resulting in a total of 4 Tmol yr^{-1}, with an uncertainty of 50% (G).

3. Results

3.1. Carbonate Dissolution in Coastal and Shelf Environments

A total of $n = 204$ data points, originating from 28 studies across 22 distinct geographic locations (Figure 1), were included in the meta-analysis (Table S3 in Supporting Information S1; $n = 67$ for coral reefs and lagoons across 13 studies; $n = 58$ for banks and bays across 5 studies; $n = 79$ for carbonate-poor shelves across 10 studies). Values for R_{diss} were included in a random-effects statistical model (Figure 2), which provided high mean dissolution rates for coral reefs and lagoons (14.9 ± 3.9 mmol m^{-2} d^{-1}) and for banks and bays with seagrass (18.8 ± 7.7 mmol m^{-2} d^{-1}), and low rates for banks and bays without seagrass (1.5 ± 2.2 mmol m^{-2} d^{-1}) and for carbonate-poor muds (1.2 ± 0.6 mmol m^{-2} d^{-1}) and sands (0.4 ± 1.8 mmol m^{-2} d^{-1}). High uncertainties were obtained for carbonate-poor sands (450% relative uncertainty) and banks and bays without seagrass (150%), while the other environments had uncertainties ≤50%. Since no data was available for carbonate-rich shelves, the dissolution rate of banks and bays without seagrass was used as a proxy for this environment, due to similarities in terms of high $CaCO_3$ content and lack of vegetation.

Q statistics indicated significant heterogeneity at the 95% significance level for coral reefs and lagoons ($Q = 28.14$, df = 12, $p = 0.005$) but not for the other environments ($Q = 1.56$, df = 3, $p = 0.668$ and $Q = 4.56$, df = 3, $p = 0.207$ for banks and bays with and without seagrass, respectively; $Q = 1.03$, df = 6, $p = 0.984$ and $Q = 4.56$, df = 3, $p = 0.207$ for carbonate-poor muds and sands, respectively). These results suggest that for coral reefs and lagoons, dissolution rates across studies differed more than expected by chance, illustrating that they are influenced by variability in environmental conditions and sampling methodology. For all other environments, the absence of significant heterogeneity suggests that a "true" dissolution rate exists (and hence implying that a fixed-effects model could be applied). However, since Q is sensitive to both the number of studies and the study precision, its significance is highly dependent on the statistical power of the meta-analysis. Therefore, in the next section, we discuss heterogeneity in relation to the parameters τ^2 and I^2 rather than relying on Q statistics (Borenstein et al., 2009).

In coral reefs and lagoons, moderate to high heterogeneity was observed ($\tau^2 = 8.35$, $I^2 = 57.4\%$), which is explained by the large geographic spread of the studies (Figure 1) and the different methods that were used to

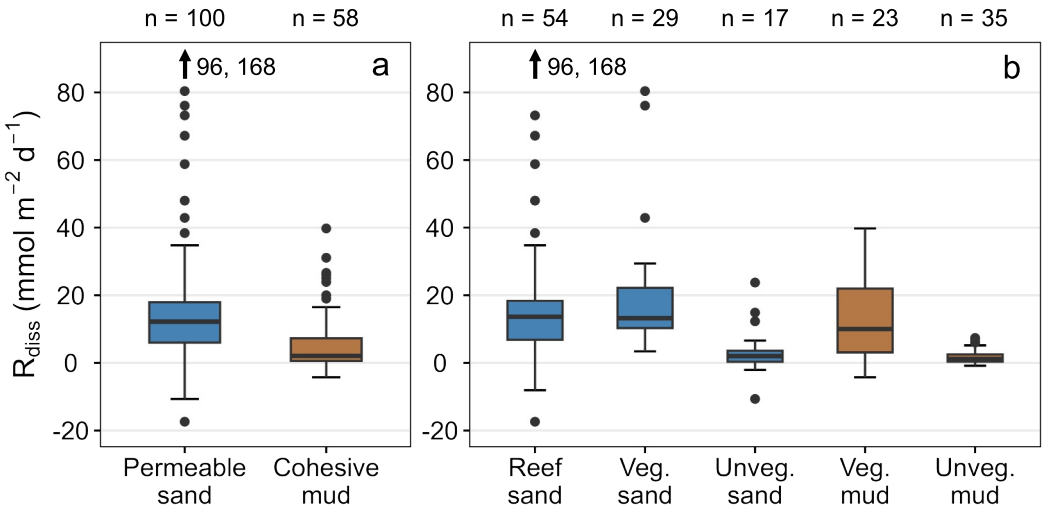

Figure 3. Boxplots showing dissolution rates (R_{diss}) for n number of data points per category. (a) Dissolution rates in permeable sands and cohesive muds. (b) Dissolution rates in reef sands, and vegetated and unvegetated sands and muds.

estimate dissolution rates (Table S1 in Supporting Information S1). Low to moderate heterogeneity was observed in banks and bays with seagrass ($\tau^2 = 15.05$, $I^2 = 0\%$) and without seagrass ($\tau^2 = 1.21$, $I^2 = 34.2\%$). The high τ^2 and low I^2 values for seagrass banks may seem counterintuitive but are explained by how the variance was calculated for individual studies. Two of the four seagrass bank studies were assigned a high, conservative variance estimate as insufficient information was available to calculate their variance (Table S3 in Supporting Information S1). This resulted in a model estimate with high within-study variance, which dominated the total variance ($I^2 = 0\%$) despite substantial between-study variance ($\tau^2 = 15.05$). Methodological differences (Table S1 in Supporting Information S1), as well as differences in sediment types, ranging from mud to sand (e.g., Burdige et al., 2008; Walter & Burton, 1990), contributed to the observed heterogeneity. Carbonate-poor muds and sands showed little to no heterogeneity ($\tau^2 = 0$, $I^2 = 0\%$ and $\tau^2 < 0.0001$, $I^2 = 34.1\%$, respectively). In this case, a fixed-effects model could have been appropriate. However, given the geographic spread of the data (Figure 1) and the heterogeneous nature of the other environments, a random-effects model was retained.

Data points were also categorized according to grain size (permeable sands and cohesive muds; Figure 3a) and grain size in combination with the presence of vegetation (Figure 3b). These parameters have a strong impact on the dissolution rates, as will be discussed in the following sections. Coral reef sands were considered separately due to their typical low organic matter content but high mineralization rates (Watanabe & Nakamura, 2019). Dissolution rates were generally higher in sands than in muds and higher in vegetated systems than in unvegetated systems.

3.2. Coastal and Shelf $CaCO_3$ Budget

Ecosystem-based dissolution rates (Table 2) were obtained by multiplying the mean areal dissolution rates derived from the model by the total area for each environment (Table 1). High dissolution rates were obtained for coral reefs and lagoons (5 ± 1 Tmol yr^{-1}; ~45% of the total coastal and shelf dissolution) and for carbonate-poor shelves (5 ± 9 Tmol yr^{-1}; ~45%), whereas banks and bays (0.6 ± 0.3 Tmol yr^{-1}; ~5%) and carbonate-rich shelves (0.7 ± 1.0 Tmol yr^{-1}; ~6%) represent minor contributions. Despite their low areal dissolution rates (Figure 2), carbonate-poor shelves represent a major component of the global coastal and shelf $CaCO_3$ budget because they cover 88% of the total area (Table 2). In contrast, banks and bays occupy a small area and therefore contribute considerably less to the global coastal and shelf budget. The total estimated dissolution rate for coastal and shelf environments is 11 ± 9 Tmol yr^{-1} (Table 2). While this rate has a high uncertainty, mostly due to the high uncertainty of carbonate-poor sand dissolution, it aligns with a previous estimate based on one-dimensional reactive transport modeling (7 Tmol yr^{-1}; Krumins et al., 2013), as well as an often cited—but coarse—estimate of ~6.5 Tmol yr^{-1} by Milliman (1993).

Table 2
Global Coastal and Shelf $CaCO_3$ Budget

Environment	Area[a] (10^{12} m^2)	Production[b] (Tmol yr^{-1})	Burial[b] (Tmol yr^{-1})	Dissolution (Tmol yr^{-1})	Additional input[b] (Tmol yr^{-1})	Residual[c] (Tmol yr^{-1})
Coral reef/lagoon	0.9	9 (G)	7 (G)	5 ± 1		
Bank/bay	0.4	2 (F)	1 (F)	0.6 ± 0.3		
Seagrass (14%)	0.06			0.4 ± 0.2		
No seagrass (86%)	0.34			0.2 ± 0.3		
Carbonate-rich shelf	1.3	4 (F)	2 (P)	0.7 ± 1.0[d]		
Carbonate-poor shelf	19.4	23 (P)	6 (G)	5 ± 9		
Mud (30%)	5.8			3 ± 1		
Sand (70%)	13.6			2 ± 9		
Total coastal/shelf	22	38 (P)	16 (F)	11 ± 9	4 (G)	15 (P)

Note. Uncertainties for dissolution rates are shown as half the 95% confidence interval. Uncertainties for other processes are shown within parentheses as G (~50% uncertainty), F (~100% uncertainty), or P (>100% uncertainty). [a]Smith and Mackenzie (2016). [b]Derivations and references are provided in the Methods section. [c]Residual was calculated as production + additional input − burial − dissolution. [d]Dissolution rate of banks and bays without seagrass was used as a proxy, see text for details. Percentage of seagrass cover in banks and bays is derived from McKenzie et al. (2020), and percentages of carbonate-poor mud and sand shelf are from Burdige (2007).

Dissolution rates were combined with production, burial, and additional input rates to arrive at a global annual coastal and shelf $CaCO_3$ budget (Table 2). Calcium carbonate enters the coastal ocean through river input and meltwater discharge and ice-rafted debris (4 Tmol yr^{-1}; 50% uncertainty) or is locally produced (38 Tmol yr^{-1}; >100% uncertainty), while it is lost through burial (16 Tmol yr^{-1}; 100% uncertainty) and dissolution in the sediment (11 ± 9 Tmol yr^{-1}). Despite several high uncertainties, especially for production in the poorly constrained carbonate-poor shelf environment, these results indicate that the $CaCO_3$ budget may not be balanced, resulting in a residual of 15 Tmol yr^{-1} (>100% uncertainty).

4. Discussion

4.1. Methodology Aspects and Data Availability

We have made an inventory of published data on areal $CaCO_3$ dissolution rates (R_{diss}), thus providing mean dissolution rates for global environments. These R_{diss} values carry a relatively high uncertainty (Figure 2), which originates from the limited number of studies as well as the different methodologies used to measure dissolution rates. Furthermore, there is a clear geographical bias in terms of study sites. Most studies on carbonate dissolution have been conducted in (sub)tropical environments, with the majority conducted in the Northern Hemisphere (Figure 1). No data were found on carbonate dissolution in carbonate-rich shelf environments, and among the major vegetated ecosystems—seagrass meadows, mangrove forests and salt marshes—data are almost exclusively limited to seagrass ecosystems. Recent efforts have investigated how mangroves and salt marshes influence coastal carbonate chemistry (see Reithmaier et al., 2023 for a synthesis), but the specific role of carbonate dissolution in the A_T production in these environments remains poorly constrained.

Additionally, many of the included studies comprise snapshot observations that fail to capture seasonal or annual variability, and data were pooled without explicitly accounting for additional environmental factors due to the limited amount of available data. Future research should target all types of marine environments, while also incorporating temporal dynamics and environmental controls, thereby providing a more comprehensive understanding of carbonate dissolution and its role in global carbonate cycling. This is particularly critical for carbonate-poor sands, as these sediments cover the largest portion of the total coastal and shelf area (62%) but have largely been overlooked in the context of $CaCO_3$ dissolution (only 4 out of a total of 28 studies). Moreover, typical in situ techniques (e.g., incubation chambers) are difficult to implement in sandy sediments due to their resistance to instrument penetration (Lunstrum & Berelson, 2022). As a result, these sediments are often collected

using grab samplers, which inherently disturb the sediment and affect sedimentary processes. Furthermore, hydrodynamic forcing, which drives pore-water advection in sands, is difficult to replicate accurately in laboratory settings, leading to artificial conditions that may not reflect in situ dissolution dynamics. Dissolution rates obtained under such conditions may therefore differ substantially from in situ rates.

4.2. Drivers of $CaCO_3$ Dissolution in Coastal and Continental Shelf Sediments

Dissolution rates obtained from literature showed substantial variability both within and between the types of coastal and shelf environments (Figure 2). In this section, we discuss the drivers of $CaCO_3$ dissolution in coastal and shelf sediments and how they are affected by environmental conditions.

Sedimentary carbonate dissolution is principally controlled by the type of $CaCO_3$ minerals present and the pore-water saturation state of the $CaCO_3$ minerals in question. Carbonates in coastal and shelf sediments are predominantly of biogenic origin, with their principal mineral phases being aragonite and a spectrum of magnesium calcites. The magnesium content of $CaCO_3$ is largely controlled by temperature, the metabolism of the calcifying organism and the mineralogic form they produce (Chave, 1954). Aragonite rarely contains over 1 mol% of magnesium, while calcite is further subdivided in low-magnesium calcite (LMC; <4 mol% $MgCO_3$) and high-magnesium calcite (HMC; >4 mol% $MgCO_3$; Haese et al., 2014). In shallow tropical and subtropical environments, such as reefs and bays, organisms that produce aragonite (e.g., scleractinian corals, green algae) and HMC (e.g., red coralline algae, benthic foraminifera) dominate, whereas on deeper shelves, sediments are dominated by the settled casts of pelagic organisms that produce LMC (e.g., planktonic coccolithophores and foraminifera; Table 1; Andersson et al., 2008; Chave, 1954, 1962; Morse & Mackenzie, 1990). HMC is generally more soluble than LMC and aragonite due to its lower thermodynamic stability (Eyre et al., 2014; Walter & Morse, 1985). Therefore, differences in dissolution rates in sediments have been suggested to partly result from variations in HMC content (Yates & Halley, 2003). In the following discussion, we use aragonite as an example, but the same reasoning holds for any phase of $CaCO_3$.

Sedimentary carbonate dissolution requires that the pore water of the sediment becomes undersaturated. The saturation state of the pore water is determined by (a) the saturation state of overlying water, (b) the rate at which overlying water is exchanged with pore water across the sediment-water interface, and (c) the rate of aerobic mineralization in the sediment (which provides carbonic acid to the pore water). If the overlying water is undersaturated, dissolution can readily proceed, as occurs in deep-sea sediments below the saturation horizon (see below). If the overlying water is oversaturated, the pore water needs an extra dose of acid from aerobic mineralization to become undersaturated. This process is generally termed metabolic carbonate dissolution (Figure 4a). Note that even when the overlying water is oversaturated, its saturation state still influences carbonate dissolution in the sediment. For the same ventilation rate, overlying waters with a higher saturation state require more aerobic mineralization to acidify the pore water for carbonate dissolution to occur. Several studies have shown that sediment incubations conducted under elevated pCO_2 conditions (i.e., reduced saturation state) resulted in higher dissolution rates compared with incubations at normal pCO_2 levels (Andersson et al., 2007, 2009; Cyronak et al., 2013b; Lunstrum & Berelson, 2022).

Metabolic carbonate dissolution is regulated by a variety of parameters in coastal and shelf sediments (Andersson & Gledhill, 2013), which can be categorized into two primary drivers: reactive organic matter content and oxygen availability (Equation 2; Figure 4b). While the respiration of organic matter with oxygen acidifies the pore water, organic matter mineralization in the absence of oxygen generates alkalinity and increases the $CaCO_3$ saturation state (Soetaert et al., 2007). Reactive organic matter is provided to the sediment by the settling of detritus from the water column or by benthic flora. Oxygen availability on the other hand is governed by a variety of processes. First, sediment grain size affects the permeability of sediments, and this controls the transport of oxygen from the oxygenated overlying water to the sediment. In fine-grained cohesive sediments, transport is restricted to molecular diffusion (Janssen et al., 2005), resulting in shallow oxygen penetration. In coarse-grained permeable sediments, pore-water advection provides an additional transport mechanism, allowing oxygen to penetrate deeper into the sediment (Huettel & Gust, 1992). A parameter closely related to advection is pore-water residence time (PRT), which is defined as the time that seawater remains in the sediment before being exchanged or flushed out. The PRT should be long enough to allow aerobic mineralization to acidify the pore water, driving it toward undersaturation and initiating $CaCO_3$ dissolution but not too long so that the pore water does not become anoxic. Sediments with higher organic matter content and thus higher mineralization rates require shorter PRTs to drive

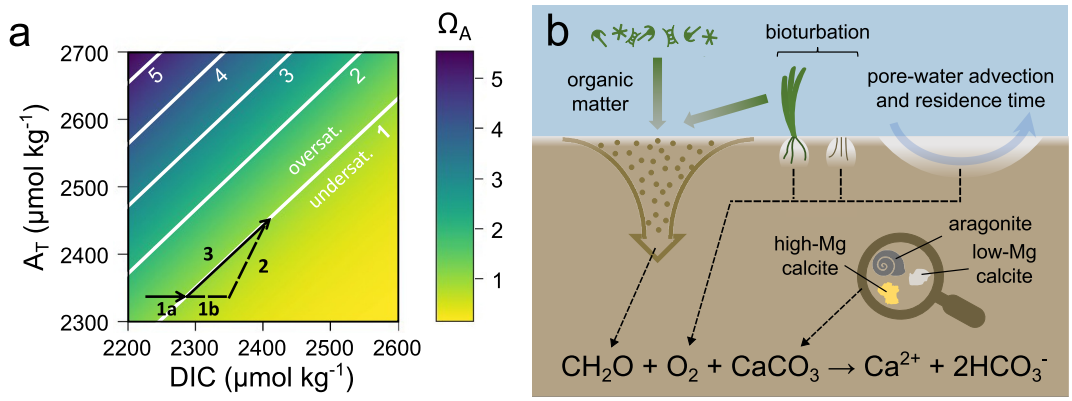

Figure 4. Metabolic carbonate ($CaCO_3$) dissolution. (a) Thermodynamic diagram. Changes of alkalinity (A_T) and dissolved inorganic carbon (DIC) are superimposed on a contour plot of the aragonite saturation state (Ω_A) at 15°C and a salinity of 35 PSU. Aerobic mineralization increases DIC according to vector 1a until saturation is reached ($\Omega_A = 1$). Beyond this point, aerobic mineralization continues (vector 1b) in concert with $CaCO_3$ dissolution (vector 2), which increases A_T and DIC in a 2:1 ratio (Equation 1). The combined reaction, metabolic $CaCO_3$ dissolution (vector 3), increases A_T and DIC in a 2:2 ratio (Equation 2). Vector 1a becomes longer as Ω_A of the overlying water increases, indicating that more aerobic respiration is required to acidify the pore water until undersaturation. (b) Parameters affecting metabolic $CaCO_3$ dissolution. Oxygen availability and reactive organic matter content are the primary drivers. Oxygen is affected by sediment grain size, and by secondary drivers such as pore-water advection, the closely related pore-water residence time, and biological processes such as bioturbation (and bio-irrigation) and oxygen release from seagrass rhizomes. Organic matter is provided to the sediment by the settling of detritus from the water column. The different $CaCO_3$ mineral phases are high-magnesium calcite, low-magnesium calcite and aragonite.

the pore water toward undersaturation (Figure 5). Finally, oxygen penetration can be enhanced through bioturbation, a process in which infaunal organisms rework the sediment, increasing permeability and facilitating fluid transport (Aller, 1980). A large fraction of these bioturbators create burrows, which they flush to bring oxygen-rich water to deeper anoxic sediment layers (Meysman et al., 2006). This process, called bio-irrigation, reoxidizes reduced metabolites in the anoxic zone (which lowers the pH; Soetaert et al., 2007) and enhances aerobic mineralization. The combined influence of all these processes explains the substantial heterogeneity in the field data, which can be further elaborated upon in the context of the different coastal and shelf environments.

4.2.1. Deep-Sea and Slope Sediments

As the $CaCO_3$ saturation state is strongly pressure- (and therefore depth-) dependent, research on $CaCO_3$ dissolution has historically targeted deep-sea and, to a lesser extent, slope sediments (Berelson et al., 2007; Wollast, 1994), while coastal and shelf sediments were often assumed to be areas of little to no dissolution (e.g., Broecker & Takahashi, 1977). In this section, only a brief overview is provided on deep-sea and slope $CaCO_3$ dissolution. We refer the reader to Berelson et al., 2007 for a more in-depth review.

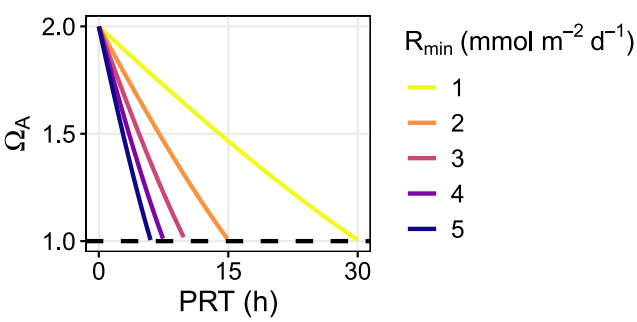

Figure 5. Pore-water aragonite saturation state (Ω_A) transition from oversaturation ($\Omega_A = 2$) to (under)saturation ($\Omega_A \leq 1$) as a function of pore-water residence time for a range of mineralization rates (R_{min}). Higher mineralization rates require shorter PRTs to reach undersaturation. Plot was made using typical seawater parameters (A_T = 2,300 µmol kg^{-1}; T = 16°C; S = 35 PSU; starting dissolved inorganic carbon concentration = 2127.3 µmol kg^{-1} to set saturation state Ω_A to 2).

In deep-sea sediments below the saturation horizon, dissolution is mainly driven by bottom water undersaturation, but can be supplemented by metabolic dissolution (Cetiner et al., 2025). However, low organic matter content in deep-sea sediments limits metabolic carbonate dissolution, as a large fraction of the organic matter is remineralized in the water column before settling onto the deep seafloor. Furthermore, transport in deep-sea sediments is primarily driven by molecular diffusion, with little contribution from advective processes (Boudreau, 1997; Boudreau et al., 2020). This further limits $CaCO_3$ dissolution, as restricted flushing of the pore water with undersaturated oxygenated bottom water leads to the accumulation of dissolution products that drives the pore water toward oversaturation.

The continental slope forms the connection between the deep sea and the continental shelf. With the exception of high-latitude environments, slope

sediments lie above the calcite saturation horizon and above the aragonite saturation horizon in the Atlantic Ocean (Milliman, 1993). $CaCO_3$ minerals in slope sediments therefore typically dissolve primarily through metabolic carbonate dissolution, either in the sediment or in settling particle aggregates. Organic matter, either obtained indirectly from lateral off-shelf transport, or directly from in situ production in the overlying water, can vary considerably in concentration due to the large depth range of slope sediments. In deeper slope sediments, the input of organic matter is low compared to shallower slope sediments, as a larger fraction is remineralized in the water column before reaching the seafloor. As a result, deep slope sediments have a lower potential for metabolic carbonate dissolution than shallow slope sediments. However, since the saturation state of the water in these deeper environments is lower, less aerobic mineralization is needed to drive the pore water toward undersaturation.

4.2.2. Shelf Sediments

Shelf sediments are typically located far above the saturation horizon of calcite and aragonite, and thus $CaCO_3$ dissolves exclusively through metabolic carbonate dissolution. Most of the dissolution occurs in the sediment, as the settling time of degrading particle aggregates is short in these shallow environments. Compared to deep-sea sediments, shelf environments receive a high organic matter input due to a high local primary production combined with land-derived organic matter. Shelf sediments are typically classified by grain size as either muddy or sandy, with each exhibiting distinct constraints on dissolution. In cohesive muddy sediments, diffusive transport leads to shallow oxygen penetration. As organic matter content regulates the CO_2 production necessary for $CaCO_3$ dissolution, higher organic matter content leads to higher mineralization and higher corresponding dissolution rates as long as oxygen remains available. Once oxygen is depleted, anaerobic mineralization processes take over, which produce alkalinity and thus inhibit dissolution. A clear example of oxygen limitation can be seen in sediments during spring blooms, where oxygen depletion and corresponding anaerobic mineralization increase the pH of the overlying water, inhibiting dissolution (Green & Aller, 2001). In permeable sandy sediments, additional advective transport leads to deeper oxygen penetration. This wider oxic zone generally leads to higher dissolution rates compared to those found in muddy sediments (Figure 3a). The observed negative values (Figure 3) may be explained by two factors. First, uncertainties in the measurements of DIC fluxes, mineralization rates, and oxygen fluxes used to derive dissolution rates may result in negative estimates. Second, a considerable number of data points were collected in situ within carbonate-rich environments characterized by high calcification activity. Although the data used in this study were restricted to dark conditions to remove the effect of calcification, some calcification may still have occurred, resulting in the negative rates.

The effect of bioturbation and bio-irrigation on oxygen penetration has been observed both in muddy shelf sediments, where shell pitting and pore-water Ca^{2+} profiles suggest higher dissolution rates in highly bioturbated areas (Aller, 1982), and in sandy shelf sediments, where the impact of bioturbation on alkalinity production was studied in core incubations with sediment before and after the addition of deep-burrowing lugworms (Rao et al., 2014). Higher alkalinity fluxes related to metabolic $CaCO_3$ dissolution were observed in the bioturbated cores. Finally, the effect of PRT on $CaCO_3$ dissolution in shelf sands has been studied through sediment incubations in which PRT was manipulated (Lunstrum & Berelson, 2022). For short PRTs, negligible dissolution was observed because the acidity produced by aerobic mineralization was flushed out before it could drive $CaCO_3$ dissolution. Once a threshold was reached, the dissolution rates increased with longer PRTs. However, as PRTs further increased, aerobic mineralization decreased due to hypoxic pore-water buildup, ultimately lowering the dissolution efficiency (Lunstrum & Berelson, 2022).

If metabolic carbonate dissolution is fully efficient, 50% of the DIC pool in the pore water should originate from organic matter mineralization and 50% from $CaCO_3$ dissolution (Equation 2). When sufficient CO_2 has been produced through aerobic mineralization to bring the pore water toward undersaturation, a 1:1 relationship is established between mineralization and dissolution, as long as oxygen is present in the sediment (Figure 6a). The dissolution efficiency is governed by the full range of environmental parameters (Figure 4b), and since these parameters vary considerably across marine environments, efficiencies can differ significantly (Figures 6b and 6c). Cohesive muds are generally more oxygen-limited, while sandy, permeable sediments are typically low in organic matter compared to muddy sediments (de Beer et al., 2005), making them more prone to organic matter limitation.

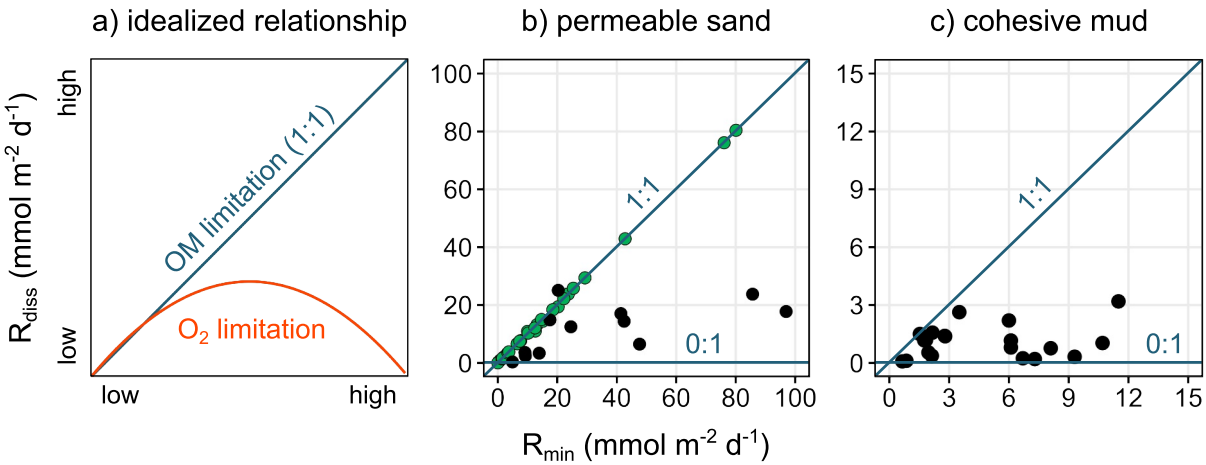

Figure 6. Dissolution rates (R_{diss}) as a function of mineralization rates (R_{min}), which serve as a proxy for reactive organic matter content. Figures only include studies where both R_{diss} and R_{in} were directly reported or derivable from supplementary data. The theoretical maximum (1:1) and minimum (0:1) dissolution efficiency is shown, as discussed in the text. (a) idealized relationship showing an organic matter (OM)-limited system (fully efficient) and a conceptual curve describing a system that shifts from OM limitation to O_2 limitation. (b) Permeable sands including data points from all environments. Green data points are from seagrass studies in which R_{diss} was calculated from dissolved inorganic carbon fluxes, assuming full efficiency. (c) Cohesive muds including data points from all environments.

4.2.3. Bank/Bay

Organic matter accumulation in banks and bays varies considerably between locations and depends on the presence of vegetation. Vegetation modulates not only local organic matter input but also oxygen transport by releasing O_2 from the rootzone (Colmer, 2003; Ku et al., 1999). In seagrass banks and bays, the combination of high organic matter content, enhanced pore-water oxygenation and large fractions of HMC from seagrass-associated organisms (e.g., mollusks, bryozoans; Table 1), makes these environments highly efficient for $CaCO_3$ dissolution, showing the highest areal dissolution rates of all coastal and shelf environments (Figure 2). A positive correlation between seagrass density and $CaCO_3$ dissolution rate has been observed in several studies (Burdige & Zimmerman, 2002; Burdige et al., 2008, 2010) and is reflected by the large variability of dissolution rates (Figures 2 and 3b). It should be noted, however, that vegetation also enhances the deposition of detrital organic matter from the water column by reducing seawater flow. This reduced flow reduces pore-water irrigation, which, in combination with enhanced detrital organic matter deposition, causes highly dense seagrass systems to shift from being organic matter-limited to oxygen-limited (Figure 6a; Burdige & Zimmerman, 2002; Burdige et al., 2008).

Unvegetated banks and bays display considerably lower dissolution rates due to the absence of vegetation-derived organic matter (Figure 2). In muddy sediments, where oxygen penetration is shallow, additional oxygen supply, either indirectly through bio-irrigation or directly via root release, is essential, alongside high organic matter input, to sustain high dissolution rates (Figure 3b).

4.2.4. Coral Reef/Lagoon

Most of the more recent studies on $CaCO_3$ dissolution in coastal sediments have targeted tropical and subtropical environments with coral reefs, in the context of ocean acidification (see, e.g., Andersson & Gledhill, 2013; Eyre et al., 2014, and references therein). Several studies suggest that reefs might transition from net accreting to net dissolving by the end of this century (Andersson & Mackenzie, 2004; Andersson et al., 2009; Eyre et al., 2018). Reef and lagoon sediments are rich in $CaCO_3$ and display high rates of organic matter mineralization (Watanabe & Nakamura, 2019). Live coral reefs produce both organic and inorganic carbon within their structure, while surrounding sediments accumulate organic and inorganic carbon through spillover from reefs. Moreover, reef and lagoon sediments are generally coarse-grained, resulting in high permeability and deep oxygen penetration. This, in combination with large fractions of HMC (Table 1), provides optimal conditins for $CaCO_3$ dissolution, leading to some of the highest areal dissolution rates in coastal and shelf environments (Figures 2 and 3b). The observed variability in dissolution rates among reefs and lagoons can be partly explained by differences in live coral cover. In highly advective reef sediments, low PRTs can become a limiting factor, if the CO_2 produced by aerobic

mineralization is flushed out before it can drive $CaCO_3$ dissolution. Chamber incubations in permeable sediments with high background flushing rates (likely resulting from bio-irrigation) show that additional advection induced by stirring motion elevated $CaCO_3$ dissolution rates until a certain threshold, after which metabolic carbonate dissolution was hampered by the lack of CO_2 buildup in the pore water (Rao et al., 2012).

4.3. The Role of Coastal and Shelf $CaCO_3$ Cycling in the Global Carbon Cycle

In this section, we discuss coastal and shelf $CaCO_3$ cycling as part of the global carbon cycle and evaluate its role in climate regulation. We find the highest dissolution rates per unit area in coral reefs and lagoons, and in vegetated banks and bays (seagrass meadows; Figure 2), due to a combination of high fractions of HMC, which dissolve faster than other $CaCO_3$ minerals, deep oxygen penetration and high organic matter respiration in the sediment. Carbonate-poor shelves, on the other hand, display much lower dissolution rates on an areal basis, but integrated over the total area, these carbonate-poor shelves become equally important as coral reefs and lagoons, due to their much larger surface area (Table 2). This is particularly noteworthy, as most research on $CaCO_3$ cycling has traditionally focused on coral reefs, while carbonate-poor shelves have been largely overlooked. This is especially the case for carbonate-poor sands, for which dissolution data are only available from 4 studies (Table S3 in Supporting Information S1), resulting in a high relative uncertainty of 450%.

Alkalinity produced by $CaCO_3$ dissolution in shallow sediments buffers climate change on much faster timescales than deep-sea sediments due to the rapid equilibration of the shallow and well-mixed coastal water column with the atmosphere (Thomas et al., 2009). Barring any secondary reactions, the dissolution of one mol of $CaCO_3$ in the sediment leads to the addition of 2 mol of A_T and 1 mol of DIC to the water column (Equation 1). We apply a 2:1 ratio, as we consider only the direct effect of $CaCO_3$ dissolution and not metabolic $CaCO_3$ dissolution. Aerobic respiration would occur irrespective of $CaCO_3$ dissolution and is therefore not included. The addition of one mol of A_T to the surface ocean at a constant pCO_2 ~400 ppm induces an average uptake of 0.84 mol of atmospheric CO_2 (Schulz et al., 2023). Therefore, the dissolution of one mol of $CaCO_3$ will lead to an additional uptake of 0.68 mol of CO_2 from the atmosphere (i.e., 2×0.84 mol from A_T addition minus 1 mol already provided by DIC). As such, we estimate that a total of 7 ± 6 Tmol of CO_2 might be sequestered annually by sedimentary $CaCO_3$ dissolution in coastal and shelf environments. The global ocean currently absorbs 242 ± 33 Tmol CO_2 yr^{-1}, representing about 26% of the total anthropogenic CO_2 emissions (Friedlingstein et al., 2025). Accordingly, sedimentary coastal and shelf $CaCO_3$ dissolution represents ~3% of the yearly global ocean CO_2 sink (1.4% coral reefs and lagoons, 0.2% banks and bays, 0.2% carbonate-rich shelves, 1.3% carbonate-poor shelves). As ocean acidification continues to reduce the calcium carbonate saturation state of the coastal seawater, one expects that this will elevate $CaCO_3$ dissolution in coastal and shelf sediments, and that CO_2 buffering in shallow sediments will further increase in the future (Eyre et al., 2014; Lunstrum & Berelson, 2022; van de Velde et al., 2026). This effect may already be underway, as several coastal and shelf areas have recently begun transitioning from CO_2 sources to sinks (Andersson & Mackenzie, 2004; Andersson et al., 2005; Chen & Borges, 2009).

Most coral reefs and lagoons are currently still sources of CO_2, as reef calcification exceeds sedimentary dissolution (Eyre et al., 2018). With progressing ocean acidification, however, reef sediments are expected to eventually shift from net precipitation to net dissolution, which is estimated to happen by the end of this century or the start of the next (Andersson, 2015). This shift would turn coral reefs and lagoons into sinks for atmospheric CO_2. Continental shelf areas are also shifting from being CO_2 sources to being CO_2 sinks (Bauer et al., 2013; Frankignoulle & Borges, 2001; Laruelle et al., 2018). Historically, respiration of land-derived organic matter and biogenic calcification made these regions net sources of CO_2 (Bauer et al., 2013; Mackenzie et al., 2004). Currently, however, enhanced physico-chemical uptake of CO_2 driven by rising atmospheric concentrations, together with increased biological uptake stimulated by anthropogenic nutrient input into the ocean, is turning continental shelves into CO_2 sinks (Bauer et al., 2013). The buffering capacity of these environments toward increasing CO_2 is dependent on the presence of sufficient $CaCO_3$ in the sediment. Increased dissolution due to ocean acidification could result in higher dissolution than calcification, which could, given enough time, eventually deplete $CaCO_3$ and result in a transition from CO_2 sink back to source (Lunstrum & Berelson, 2022). Assuming a 1% excess of dissolution over the current precipitation rate of 23 Tmol yr^{-1} (Table 2) and a carbonate content of 1 wt.% in carbonate-poor shelf sediments, complete depletion of $CaCO_3$ in the oxic layer of carbonate-poor muddy and sandy sediments would occur within approximately 400 and 1,400 years, respectively (see Text S1 in Supporting Information S1 for calculation). However, sustained excess dissolution would also increase the

Table 3
Global Marine Calcium Carbonate ($CaCO_3$) Budget

Environment	Area (10^{12} m^2)	Production (Tmol yr^{-1})	Burial (Tmol yr^{-1})	Dissolution (Tmol yr^{-1})	Additional input (Tmol yr^{-1})	Residual (Tmol yr^{-1})
Total coastal/shelf	22	38 (P)	16 (F)	11 ± 9	4 (G)	+15 (P)
Slope	32[a]	13 (G)[a]	6 (F)[b,c]	8 (G)[a]		−1 (P)
Water column		13 (G)	0	?		
Sediment		0	6 (F)	?		
Deep sea	308[a]	120 (G)[a]	9 (G)[d]	114 (G)[a]		−3 (P)
Water column		120 (G)	0	81 (G)		
Sediment		0	9 (G)	33 (G)		
Total slope/deep sea	340	133 (G)	15 (G)	122 (G)		−4 (P)
Total ocean	362	171 (?)	31 (?)	133 (G)	4 (G)	+11 (?)

Note. Slope and deep-sea production refers to production in the surface water above these environments. [a]Berelson et al. (2007). [b]van Weering et al. (1998). [c]Milliman and Droxler (1996). [d]Catubig et al. (1998); see Text S3 in Supporting Information S1 for derivations.

alkalinity and $CaCO_3$ saturation state of seawater, exerting a negative feedback on dissolution, which would make this $CaCO_3$ depletion scenario unlikely.

Our coastal and shelf $CaCO_3$ budget shows a residual rate of 15 Tmol yr^{-1} (>100% uncertainty; Table 2), which implies either inaccuracies in the averaged rate estimates or a lateral $CaCO_3$ export from the shelf toward the slopes and deep sea. The most uncertain component in the budget is the $CaCO_3$ production term (uncertainty >100%), for which we applied a substantial upward correction following Smith and Mackenzie (2016). This revised estimate was based on an average rate, stemming from a very wide range of values, and the contribution of other calcifying organisms was included based on estimates without direct observational data. A production overestimate could therefore partly account for the residual. On the other hand, our budget does not include $CaCO_3$ input from coastal erosion of $CaCO_3$ rocks, which has recently been identified as a significant source to coastal waters (Scholz et al., 2025; Wallmann et al., 2022). If $CaCO_3$ input from either erosion or production is indeed large, it would require significantly higher burial or dissolution rates to balance the coastal and shelf budgets. However, since both burial and dissolution have uncertainties of around 100%, they would only substantially affect the budget imbalance if they occurred at the upper edge of the uncertainty range (Table 2). It is therefore plausible that a considerable fraction of the residual rate is represented by lateral off-shelf $CaCO_3$ export. Although little to no data on export exist, we provide an order-of-magnitude estimate using a study on off-shelf particulate matter export in the Gulf of Lyon (Ferré et al., 2008) as a reference case. Assuming a $CaCO_3$ content of 70% and 1% in carbonate-rich and carbonate-poor shelf sediments, respectively, this comparison yields a total shelf export rate of 6 Tmol yr^{-1}, corresponding to ∼40% of the residual rate (see Text S2 in Supporting Information S1 for detailed calculation). This illustrates the plausibility of substantial lateral exports, yet its global magnitude remains highly uncertain due to rate uncertainties, especially for $CaCO_3$ production and coastal erosion.

Table 3 and Figure 7a show the global annual $CaCO_3$ budget, including a lateral off-shelf export of 15 Tmol yr^{-1}, as suggested by our coastal and shelf budget (Table 2), and slope and deep-sea production, burial and dissolution rates from the literature (see Text S3 in Supporting Information S1 for derivations). Slope and deep-sea dissolution rates are estimated at 8 and 114 Tmol yr^{-1}, respectively, each with an uncertainty of around 50%. Based on these estimates, coastal and shelf $CaCO_3$ dissolution may account for ∼8% of the global ocean $CaCO_3$ dissolution. Despite high uncertainty, this contribution is substantial considering that coastal and shelf environments only represent ∼6% of the global ocean surface area and that the water column is oversaturated for the $CaCO_3$ mineral phases, as compared to the undersaturated deep sea. The global budget reveals a $CaCO_3$ surplus of 11 Tmol yr^{-1} (>100% uncertainty). While such an excess might suggest that the ocean is not in a steady state, one expects a $CaCO_3$ deficit rather than a surplus, as ongoing ocean acidification has increased carbonate dissolution rates. We therefore attribute this imbalance primarily to uncertainties in rate estimates within the carbonate cycle. Besides uncertainties in coastal and shelf rates, which have already been discussed, slope burial contains the highest uncertainty in the budget (100%). The rate used in our budget (6 Tmol yr^{-1}; Table 3) is based on the poorly constrained estimate reported in Milliman and Droxler (1996). In an effort to further constrain this value, we

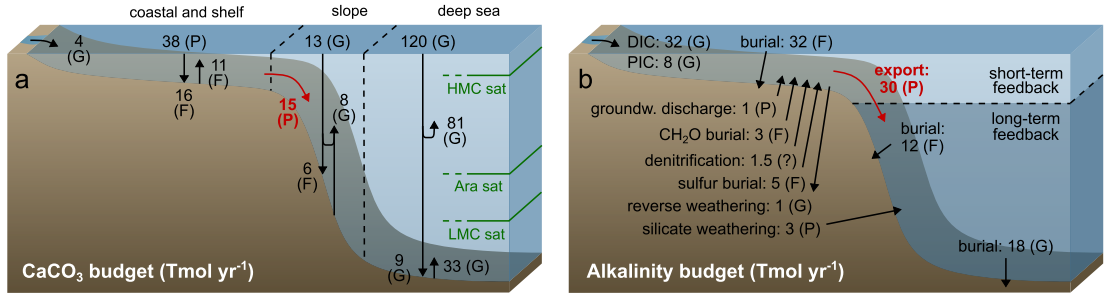

Figure 7. (a) Global marine calcium carbonate ($CaCO_3$) budget. Rates are from Tables 2 and 3 and are discussed in the main text. (b) Alkalinity budget, adapted from Middelburg et al. (2020; see Text S4 in Supporting Information S1 for derivations; updated values for $CaCO_3$ burial are discussed in the main text). Uncertainties for all processes are shown within parentheses as G (~50% uncertainty), F (~100% uncertainty), or P (more than 100% uncertainty). Reference saturation horizons for high-Mg calcite (HMC), aragonite (Ara), and low-Mg calcite (LMC) are shown in green. Rates shown in red were derived from mass balance calculations and are therefore unconstrained.

examined the available literature on slope burial but found only a single additional study (van Weering et al., 1998; Text S3 in Supporting Information S1), underscoring the large uncertainty associated with this term. A higher slope burial rate could partly resolve the budget imbalance, yet it is evident from the uncertainties observed across several of the carbonate process estimates that targeted research is needed to further refine the global $CaCO_3$ budget.

Finally, we present an updated global ocean A_T budget (Table 4, Figure 7b) adapted from Middelburg et al. (2020; see Text S4 in Supporting Information S1 for derivations and updates). The largest net source of ocean A_T is riverine (32 Tmol yr^{-1}; 50% uncertainty) through which A_T generated by continental weathering on land is delivered. River A_T estimates were derived from river DIC, assuming that bicarbonate is the predominant DIC species in rivers (Raymond & Hamilton, 2018), and that bicarbonate concentrations are equivalent to A_T (Suchet et al., 2003). The largest net sink of ocean A_T is $CaCO_3$ burial (62 Tmol yr^{-1}; 100% uncertainty). During calcification, A_T is consumed (Equation 1), and the formed $CaCO_3$ either dissolves, restoring the originally consumed A_T, or is buried, leading to a net A_T sink. The internal cycling of $CaCO_3$ via precipitation and dissolution thus underscores the important role of $CaCO_3$ dynamics in regulating climate, both on short timescales in coastal and shelf environments, and on long timescales in the deep sea.

Table 4
Global Alkalinity Budget, Adapted From Middelburg et al. (2020; See Text S4 in Supporting Information S1 for Derivations)

Alkalinity source/sink	Tmol yr^{-1}
Riverine DIC	32 (G)
Riverine PIC	8 (G)[a]
Submarine groundwater discharge	1 (P)
Organic matter burial	3 (F)
Denitrification	1.5 (?)
Sulfur burial	5 (F)
Submarine silicate weathering	3 (P)
Total sources	54 (?)
Coastal/shelf $CaCO_3$ burial	32 (F)[a]
Slope $CaCO_3$ burial	12 (F)[a]
Deep-sea $CaCO_3$ burial	18 (G)[a]
Reverse weathering	1 (G)
Total sinks	63 (F)[a]
Imbalance	−10 (?)[a]

[a]Updated values, as discussed in the main text and Text S4 in Supporting Information S1. Uncertainties for all processes are shown within parentheses as G (~50% uncertainty), F (~100% uncertainty), or P (>100% uncertainty).

Our A_T budget reveals an imbalance of −10 Tmol yr^{-1} (unknown uncertainty; Table 4), which suggests a substantial missing A_T source. However, of all the other processes contributing to the ocean A_T budget, submarine groundwater discharge carries a very high uncertainty (>100%; Table 4). A recent study reported estimates for the groundwater discharge flux ranging from 7.4 to 83 Tmol A_T yr^{-1} (Zhang & Planavsky, 2020). Such variability could easily resolve the imbalance, highlighting that future work is needed to better constrain the global A_T budget. Finally, while coastal erosion of $CaCO_3$ was not included in our budget, it is unlikely that this process would resolve the imbalance, since adding it would require an equivalent increase in $CaCO_3$ burial (e.g., in the poorly constrained slope burial) to balance the $CaCO_3$ budget, thus resulting in no net effect on the A_T budget. Instead, it is more likely that some of the other A_T sources are underestimated, particularly the poorly constrained submarine groundwater discharge.

Our $CaCO_3$ budget suggests that a considerable fraction of the coastal and shelf $CaCO_3$ is transported from the short-term (annual-decadal timescales) to the long-term (millennial timescales) carbonate cycle (Figure 7a), thus losing its short-term buffering capacity. As the exported $CaCO_3$ dissolves in deeper waters, the produced A_T will become part of the deep ocean alkalinity cycle (Figure 7b), only buffering atmospheric CO_2 on millennial timescales (Archer, 1996).

5. Summary and Outlook

In this study, we compiled carbonate dissolution rates and discussed the drivers of dissolution across a range of coastal and shelf environments. Oxygenated sediments with high organic matter input and high fractions of high-magnesium calcite display the highest $CaCO_3$ dissolution rates. Our meta-analysis estimated a coastal and shelf $CaCO_3$ dissolution rate that falls within the range of literature estimates, and the associated residual was suggested to be primarily lateral off-shelf export. While sedimentary coastal and shelf dissolution has the potential to buffer a substantial amount of the global oceanic CO_2 sink on short timescales, off-shelf export transports a significant fraction of the coastal and shelf $CaCO_3$ from the short-term to the long-term CO_2 feedback.

Our study reveals three major sources of uncertainty in coastal and shelf carbonate dissolution that should be prioritized in future research to refine the $CaCO_3$ budget:

1. Carbonate-poor sands appear to play a significant role in carbonate dissolution. However, these sediments have traditionally been understudied, thus yielding large uncertainty on their total dissolution rate. Dedicated efforts are therefore needed, including the development of in situ measurement techniques suitable for coarse, permeable sediments.
2. Carbonate-rich shelf sediments as well as mangrove and salt marsh ecosystems also remain poorly constrained due to a lack of data. Although they cover smaller areas than carbonate-poor shelves, their contribution to the coastal and shelf $CaCO_3$ budget remains largely unknown and requires dedicated assessment.
3. Lateral export of $CaCO_3$ from the continental shelf might constitute a substantial component of our budget; however, this idea remains unvalidated due to a lack of empirical studies. Dedicated research is needed to quantify export rates and elucidate the underlying transport mechanisms.

Addressing these knowledge gaps is critical for validating and improving the coastal and shelf $CaCO_3$ budget.

Conflict of Interest

The authors declare no conflicts of interest relevant to this study.

Availability Statement

The data used in this study were obtained from the literature and analyzed using R Statistical Software (v.4.4.1; R Core Team, 2024). The raw data file and R script are publicly available on GitHub and archived on Zenodo at https://doi.org/10.5281/zenodo.17345835 (Goossens, 2025).

Acknowledgments
Cedric Goossens was supported by the RV/21/DEHEAT project from the Belgian Science Policy Office (BELSPO) and a University Research Fund (BOF) of the University of Antwerp. Sebastiaan J. van de Velde acknowledges the New Zealand MBIE Strategic Science Investment Fund for support via the NIWA Ocean-Climate Interaction programme. Filip J. R. Meysman was supported by the Strategic Basic Research (SBO) project (no. S000619N) from Research Foundation Flanders (FWO) and the Blue Cluster project (project no. HBC.2023.0496) from Flanders Innovation & Entrepreneurship (VLAIO).

References

Aller, R. C. (1980). Quantifying solute distributions in the bioturbated zone of marine sediments by defining an average microenvironment. *Geochimica et Cosmochimica Acta*, *44*(12), 1955–1965. https://doi.org/10.1016/0016-7037(80)90195-7

Aller, R. C. (1982). Carbonate dissolution in nearshore terrigenous muds: The role of physical and biological reworking. *Journal of Geology*, *90*(1), 79–95. https://doi.org/10.1086/628652

Aller, R. C., & Yingst, J. Y. (1985). Effects of the marine deposit-feeders *Heteromastus filiformis* (Polychaeta), *Macoma balthica* (Bivalvia), and *Tellina texana* (Bivalvia) on averaged sedimentary solute transport, reaction rates, and microbial distributions. *Journal of Marine Research*, *43*(3), 615–645. https://doi.org/10.1357/002224085788440349

Andersson, A. J. (2015). A fundamental paradigm for coral reef carbonate sediment dissolution. *Frontiers in Marine Science*, *2*. https://doi.org/10.3389/fmars.2015.00052

Andersson, A. J., Bates, N. R., & Mackenzie, F. T. (2007). Dissolution of carbonate sediments under rising pCO_2 and ocean acidification: Observations from Devil's Hole, Bermuda. *Aquatic Geochemistry*, *13*(3), 237–264. https://doi.org/10.1007/s10498-007-9018-8

Andersson, A. J., & Gledhill, D. (2013). Ocean acidification and coral reefs: Effects on breakdown, dissolution, and net ecosystem calcification. *Annual Review of Marine Science*, *5*(1), 321–348. https://doi.org/10.1146/annurev-marine-121211-172241

Andersson, A. J., Kuffner, I. B., Mackenzie, F. T., Jokiel, P. L., Rodgers, K. S., & Tan, A. (2009). Net loss of $CaCO_3$ from a subtropical calcifying community due to seawater acidification: Mesocosm-scale experimental evidence. *Biogeosciences*, *6*(8), 1811–1823. https://doi.org/10.5194/bg-6-1811-2009

Andersson, A. J., & Mackenzie, F. T. (2004). Shallow-water oceans: A source or sink of atmospheric CO_2? *Frontiers in Ecology and the Environment*, *2*(7), 348–353. https://doi.org/10.1890/1540-9295(2004)002[0348:soasos]2.0.co;2

Andersson, A. J., Mackenzie, F. T., & Bates, N. R. (2008). Life on the margin: Implications of ocean acidification on Mg-calcite, high latitude and cold-water marine calcifiers. *Marine Ecology Progress Series*, *373*, 265–273. https://doi.org/10.3354/meps07639

Andersson, A. J., Mackenzie, F. T., & Lerman, A. (2005). Coastal ocean and carbonate systems in the high CO_2 world of the Anthropocene. *American Journal of Science*, *305*(9), 875–918. https://doi.org/10.2475/ajs.305.9.875

Archer, D. (1996). A data-driven model of the global calcite lysocline. *Global Biogeochemical Cycles*, *10*(3), 511–526. https://doi.org/10.1029/96GB01521

Bach, L. T. (2024). The additionality problem of ocean alkalinity enhancement. *Biogeosciences*, *21*(1), 261–277. https://doi.org/10.5194/bg-21-261-2024

Balch, W., Drapeau, D., Bowler, B., & Booth, E. (2007). Prediction of pelagic calcification rates using satellite measurements. *Deep Sea Research Part II: Topical Studies in Oceanography*, *54*(5–7), 478–495. https://doi.org/10.1016/j.dsr2.2006.12.006

Bauer, J. E., Cai, W.-J., Raymond, P. A., Bianchi, T. S., Hopkinson, C. S., & Regnier, P. A. G. (2013). The changing carbon cycle of the coastal ocean. *Nature*, *504*(7478), 61–70. https://doi.org/10.1038/nature12857

Berelson, W. M., Balch, W. M., Najjar, R., Feely, R. A., Sabine, C., & Lee, K. (2007). Relating estimates of $CaCO_3$ production, export, and dissolution in the water column to measurements of $CaCO_3$ rain into sediment traps and dissolution on the sea floor: A revised global carbonate budget. *Global Biogeochemical Cycles*, *21*(1). https://doi.org/10.1029/2006GB002803

Borenstein, M., Hedges, L. V., Higgins, J. P. T., & Rothstein, H. R. (2009). Identifying and quantifying heterogeneity. In *Introduction to meta-analysis* (pp. 107–125). John Wiley & Sons Ltd. https://doi.org/10.1002/9780470743386

Boudreau, B. P. (1997). *Diagenetic models and their implementation: Modelling transport and reactions in aquatic sediments*. Springer-Verlag. https://doi.org/10.1007/978-3-642-60421-8

Boudreau, B. P., Middelburg, J. J., & Luo, Y. (2018). The role of calcification in carbonate compensation. *Nature Geoscience*, *11*(12), 894–900. https://doi.org/10.1038/s41561-018-0259-5

Boudreau, B. P., Sulpis, O., & Mucci, A. (2020). Control of $CaCO_3$ dissolution at the deep seafloor and its consequences. *Geochimica et Cosmochimica Acta*, *268*, 90–106. https://doi.org/10.1016/j.gca.2019.09.037

Broecker, W. S., & Takahashi, T. (1977). Neutralization of fossil fuel CO_2 by marine calcium carbonate. In N. R. Anderson & A. Malahoff (Eds.), *The fate of fossil fuel CO_2 in the oceans* (pp. 213–241). Plenum Press.

Burdige, D. J., Hu, X., & Zimmerman, R. C. (2010). The widespread occurrence of coupled carbonate dissolution/reprecipitation in surface sediments on the Bahamas Bank. *American Journal of Science*, *310*(6), 492–521. https://doi.org/10.2475/06.2010.03

Burdige, D. J. (2007). Preservation of organic matter in marine sediments: Controls, mechanisms, and an imbalance in sediment organic carbon budgets? *Chemical Reviews*, *107*(2), 467–485. https://doi.org/10.1021/cr050347q

Burdige, D. J., & Zimmerman, R. C. (2002). Impact of sea grass density on carbonate dissolution in Bahamian sediments. *Limnology and Oceanography*, *47*(6), 1751–1763. https://doi.org/10.4319/lo.2002.47.6.1751

Burdige, D. J., Zimmerman, R. C., & Hu, X. (2008). Rates of carbonate dissolution in permeable sediments estimated from pore-water profiles: The role of sea grasses. *Limnology and Oceanography*, *53*(2), 549–565. https://doi.org/10.4319/lo.2008.53.2.0549

Catubig, N. R., Archer, D. E., Francois, R., deMenocal, P., Howard, W., & Yu, E. (1998). Global deep-sea burial rate of calcium carbonate during the Last Glacial Maximum. *Paleoceanography*, *13*(3), 298–310. https://doi.org/10.1029/98PA00609

Cetiner, J. E. P., Berelson, W. M., Rollins, N. E., Liu, X., Pavia, F. J., Waldeck, A. R., et al. (2025). Carbonate dissolution fluxes in deep-sea sediments as determined from in situ porewater profiles in a transect across the saturation horizon. *Geochimica et Cosmochimica Acta*, *390*, 145–159. https://doi.org/10.1016/j.gca.2024.11.027

Chave, K. E. (1954). Aspects of the biogeochemistry of magnesium 1. Calcareous marine organisms. *The Journal of Geology*, *3*(62), 266–283. https://doi.org/10.1086/626162

Chave, K. E. (1962). Factors influencing the mineralogy of carbonate sediments. *Limnology and Oceanography*, *7*(2), 218–223. https://doi.org/10.4319/lo.1962.7.2.0218

Chen, C.-T. A., & Borges, A. V. (2009). Reconciling opposing views on carbon cycling in the coastal ocean: Continental shelves as sinks and near-shore ecosystems as sources of atmospheric CO_2. *Deep Sea Research Part II: Topical Studies in Oceanography*, *56*(8–10), 578–590. https://doi.org/10.1016/j.dsr2.2009.01.001

Colmer, T. D. (2003). Long-distance transport of gases in plants: A perspective on internal aeration and radial oxygen loss from roots. *Plant, Cell & Environment*, *26*(1), 17–36. https://doi.org/10.1046/j.1365-3040.2003.00846.x

Cyronak, T., Santos, I. R., & Eyre, B. D. (2013b). Permeable coral reef sediment dissolution driven by elevated pCO_2 and pore water advection. *Geophysical Research Letters*, *40*(18), 4876–4881. https://doi.org/10.1002/grl.50948

Dean, C. L., Harvey, E. L., Johnson, M. D., & Subhas, A. V. (2024). Microzooplankton grazing on the coccolithophore Emiliania huxleyi and its role in the global calcium carbonate cycle. *Sciences Advances*, *10*(45), eadr5453. https://doi.org/10.1126/sciadv.adr5453

de Beer, D., Wenzhöfer, F., Ferdelman, T. G., Boehme, S. E., Huettel, M., Van Beusekom, J. E. E., et al. (2005). Transport and mineralization rates in North Sea sandy intertidal sediments, Sylt-Rømø Basin, Wadden Sea. *Limnology and Oceanography*, *50*(1), 113–127. https://doi.org/10.4319/lo.2005.50.1.0113

Durán, R., & Guillén, J. (2018). Continental shelf landforms. In *Submarine geomorphology* (pp. 185–206). https://doi.org/10.1007/978-3-319-57852-1_11

Eyre, B. D., Andersson, A. J., & Cyronak, T. (2014). Benthic coral reef calcium carbonate dissolution in an acidifying ocean. *Nature Climate Change*, *4*(11), 969–976. https://doi.org/10.1038/nclimate2380

Eyre, B. D., Cyronak, T., Drupp, P., De Carlo, E. H., Sachs, J. P., & Andersson, A. J. (2018). Coral reefs will transition to net dissolving before end of century. *Science*, *359*(6378), 908–911. https://doi.org/10.1126/science.aao1118

Falter, J. L., Lowe, R. J., Zhang, Z., & McCulloch, M. (2013). Physical and biological controls on the carbonate chemistry of coral reef waters: Effects of metabolism, wave forcing, sea level, and geomorphology. *PLoS One*, *8*(1), e53303. https://doi.org/10.1371/journal.pone.0053303

Ferré, B., Durrieu de Madron, X., Estournel, C., Ulses, C., & Le Corre, G. (2008). Impact of natural (waves and currents) and anthropogenic (trawl) resuspension on the export of particulate matter to the open ocean. *Continental Shelf Research*, *28*(15), 2071–2091. https://doi.org/10.1016/j.csr.2008.02.002

Frankignoulle, M., & Borges, A. V. (2001). European continental shelf as a significant sink for atmospheric carbon dioxide. *Global Biogeochemical Cycles*, *15*(3), 569–576. https://doi.org/10.1029/2000GB001307

Friedlingstein, P., O'Sullivan, M., Jones, M. W., Andrew, R. M., Hauck, J., Landschützer, P., et al. (2025). Global Carbon Budget 2024. *Earth System Science Data*, *17*(3), 965–1039. https://doi.org/10.5194/essd-17-965-2025

Goossens, C. (2025). Data and R Script on $CaCO_3$ Dissolution (Version v1) [Collection] [Dataset]. *Zenodo*. https://doi.org/10.5281/zenodo.17345835

Green, M. A., & Aller, R. C. (2001). Early diagenesis of calcium carbonate in Long Island Sound sediments: Benthic fluxes of Ca^{2+} and minor elements during seasonal periods of net dissolution. *Journal of Marine Research*, *59*(5), 769–794. https://doi.org/10.1357/002224001762674935

Gust, G., & Harrison, J. T. (1981). Biological pumps at the sediment-water interface: Mechanistic evaluation of the alpheid shrimp *Alpheus mackayi* and its irrigation pattern. *Marine Biology*, *64*(1), 71–78. https://doi.org/10.1007/BF00394082

Haese, R. R., Smith, J., Weber, R., & Trafford, J. (2014). High-magnesium calcite dissolution in tropical continental shelf sediments controlled by ocean acidification. *Environmental Science and Technology*, *48*(15), 8522–8528. https://doi.org/10.1021/es501564q

Harris, P. T., & Macmillan-Lawler, M. (2016). Global overview of continental shelf geomorphology based on the SRTM30_PLUS 30-Arc second database. In *Seafloor mapping along continental shelves: Research and techniques for visualizing benthic environments* (Vol. 13, pp. 169–190). Springer. https://doi.org/10.1007/978-3-319-25121-9_7

Higgins, J. P. T., Thompson, S. G., Deeks, J. J., & Altman, D. G. (2003). Measuring inconsistency in meta-analyses. *BMJ*, *327*(7414), 557–560. https://doi.org/10.1136/bmj.327.7414.557

Huettel, M., & Gust, G. (1992). Impact of bioroughness on interfacial solute exchange in permeable sediments. *Marine Ecology Progress Series*, *89*, 253–267. https://doi.org/10.3354/meps089253

Huettel, M., & Rusch, A. (2000). Advective particle transport into permeable sediments—Evidence from experiments in an intertidal sandflat. *Limnology and Oceanography*, *45*(3), 525–533. https://doi.org/10.4319/lo.2000.45.3.0525

Iglesias-Rodriguez, M. D., Armstrong, R., Feely, R., Hood, R., Kleypas, J., Milliman, J. D., et al. (2002). Progress made in study of ocean's calcium carbonate budget. *Eos*, *83*(34), 365–375. https://doi.org/10.1029/2002EO000267

Janssen, F., Huettel, M., & Witte, U. (2005). Pore-water advection and solute fluxes in permeable marine sediments (II): Benthic respiration at three sandy sites with different permeabilities (German Bight, North Sea). *Limnology and Oceanography*, *50*(3), 779–792. https://doi.org/10.4319/lo.2005.50.3.0779

Jørgensen, B. B., Wenzhöfer, F., Egger, M., & Glud, R. N. (2022). Sediment oxygen consumption: Role in the global marine carbon cycle. *Earth-Science Reviews*, *228*, 103987. https://doi.org/10.1016/j.earscirev.2022.103987

Kleypas, J. A. (2011). Ocean acidification, effects on calcification. In D. Hopley (Ed.), *Encyclopedia of modern coral reefs* (1st ed., pp. 733–737). Springer. https://doi.org/10.1007/978-90-481-2639-2_118

Krumins, V., Gehlen, M., Arndt, S., Van Cappellen, P., & Regnier, P. (2013). Dissolved inorganic carbon and alkalinity fluxes from coastal marine sediments: Model estimates for different shelf environments and sensitivity to global change. *Biogeosciences*, *10*(1), 371–398. https://doi.org/10.5194/bg-10-371-2013

Ku, T. C. W., Walter, L. M., Coleman, M. L., Blake, R. E., & Martini, A. M. (1999). Coupling between sulfur recycling and syndepositional carbonate dissolution: Evidence from oxygen and sulfur isotope composition of pore water sulfate, South Florida Platform, U.S.A. *Geochimica et Cosmochimica Acta*, *63*(17), 2529–2546. https://doi.org/10.1016/S0016-7037(99)00115-5

Laruelle, G. G., Cai, W.-J., Hu, X., Gruber, N., Mackenzie, F. T., & Regnier, P. (2018). Continental shelves as a variable but increasing global sink for atmospheric carbon dioxide. *Nature Communications*, *9*(1), 454. https://doi.org/10.1038/s41467-017-02738-z

Lebrato, M., Iglesias-Rodríguez, D., Feely, R. A., Greeley, D., Jones, D. O. B., Suarez-Bosche, N., et al. (2010). Global contribution of echinoderms to the marine carbon cycle: $CaCO_3$ budget and benthic compartments. *Ecological Monographs*, *80*(3), 441–467. https://doi.org/10.1890/09-0553.1

Lunstrum, A., & Berelson, W. M. (2022). $CaCO_3$ dissolution in carbonate-poor shelf sands increases with ocean acidification and porewater residence time. *Geochimica et Cosmochimica Acta*, *329*, 168–184. https://doi.org/10.1016/j.gca.2022.04.031

Mackenzie, F. T., Lerman, A., & Andersson, A. J. (2004). Past and present of sediment and carbon biogeochemical cycling models. *Biogeosciences*, *1*(1), 11–32. https://doi.org/10.5194/bg-1-11-2004

McKenzie, L. J., Nordlund, L. M., Jones, B. L., Cullen-Unsworth, L. C., Roelfsema, C., & Unsworth, R. K. F. (2020). The global distribution of seagrass meadows. *Environmental Research Letters*, *15*(7), 074041. https://doi.org/10.1088/1748-9326/ab7d06

Meysman, F. J. R., Galaktionov, O. S., Gribsholt, B., & Middelburg, J. J. (2006). Bioirrigation in permeable sediments: Advective pore-water transport induced by burrow ventilation. *Limnology and Oceanography*, *51*(1), 142–156. https://doi.org/10.4319/lo.2006.51.1.0142

Middelburg, J. J., Soetaert, K., & Hagens, M. (2020). Ocean alkalinity, buffering and biogeochemical processes. *Reviews of Geophysics*, *58*(3), e2019RG000681. https://doi.org/10.1029/2019RG000681

Millero, F. J. (2007). The marine inorganic carbon cycle. *Chemical Reviews*, *107*(2), 308–341. https://doi.org/10.1021/cr0503557

Milliman, J. D. (1993). Production and accumulation of calcium carbonate in the ocean: Budget of a nonsteady state. *Global Biogeochemical Cycles*, *7*(4), 927–957. https://doi.org/10.1029/93GB02524

Milliman, J. D., & Droxler, A. W. (1996). Neritic and pelagic carbonate sedimentation in the marine environment: Ignorance is not bliss. *Geologische Rundschau*, *85*(3), 496–504. https://doi.org/10.1007/bf02369004

Morse, J. W., & Mackenzie, F. T. (1990). *Geochemistry of sedimentary carbonates*. Elsevier.

Müller, G., Börker, J., Sluijs, A., & Middelburg, J. J. (2022). Detrital carbonate minerals in Earth's element cycles. *Global Biogeochemical Cycles*, *36*(5), e2021GB007231. https://doi.org/10.1029/2021GB007231

Oschlies, A., Bach, L. T., Rickaby, R. E. M., Satterfield, T., Webb, R., & Gattuso, J.-P. (2023). Climate targets, carbon dioxide removal, and the potential role of ocean alkalinity enhancement. *State of the Planet*, *2-oae2023*, 1–9. https://doi.org/10.5194/sp-2-oae2023-1-2023

Rao, A. M. F., Malkin, S. Y., Montserrat, F., & Meysman, F. J. R. (2014). Alkalinity production in intertidal sands intensified by lugworm bioirrigation. *Estuarine, Coastal and Shelf Science*, *148*, 36–47. https://doi.org/10.1016/j.ecss.2014.06.006

Rao, A. M. F., Polerecky, L., Ionescu, D., Meysman, F. J. R., & de Beer, D. (2012). The influence of pore-water advection, benthic photosynthesis, and respiration on calcium carbonate dynamics in reef sands. *Limnology and Oceanography*, *57*(3), 809–825. https://doi.org/10.4319/lo.2012.57.3.0809

Raymond, P. A., & Hamilton, S. K. (2018). Anthropogenic influences on riverine fluxes of dissolved inorganic carbon to the oceans. *Limnology and Oceanography Letters*, *3*(3), 143–155. https://doi.org/10.1002/lol2.10069

R Core Team. (2024). R: A language and environment for statistical computing. R Foundation for Statistical Computing (v. 4.4.1).

Reithmaier, G. M. S., Cabral, A., Akhand, A., Bogard, M. J., Borges, A. V., Bouillon, S., et al. (2023). Carbonate chemistry and carbon sequestration driven by inorganic carbon outwelling from mangroves and saltmarshes. *Nature Communications*, *14*(1), 8196. https://doi.org/10.1038/s41467-023-44037-w

Renforth, P., & Henderson, G. (2017). Assessing ocean alkalinity for carbon sequestration. *Reviews of Geophysics*, *55*(3), 636–674. https://doi.org/10.1002/2016RG000533

Ridgwell, A., & Zeebe, R. E. (2005). The role of the global carbonate cycle in the regulation and evolution of the Earth system. *Earth and Planetary Science Letters*, *234*(3–4), 299–315. https://doi.org/10.1016/j.epsl.2005.03.006

Riedl, R. J., Huang, N., & Machan, R. (1972). The subtidal pump: A mechanism of interstitial water exchange by wave action. *Marine Biology*, *13*(3), 210–221. https://doi.org/10.1007/BF00391379

Sarmiento, J. L., & Gruber, N. (2006). *Ocean biogeochemical dynamics*. Princeton University Press. https://doi.org/10.1063/1.2754608

Schneider, R. R., & Schulz, H. D. (2016). Marine carbonates: Their formation and destruction. In *Marine geochemistry* (pp. 283–307). https://doi.org/10.1007/3-540-32144-6_9

Scholz, F., Börker, J., Vogt, C., Hartmann, J., & Wallmann, K. (2025). Natural ocean alkalinization through erosion of glacial till and weathering at the seafloor. *Communications Earth & Environment*, *6*(1), 974. https://doi.org/10.1038/s43247-025-03009-2

Schulz, K. G., Bach, L. T., & Dickson, A. G. (2023). Seawater carbonate chemistry considerations for ocean alkalinity enhancement research: Theory, measurements, and calculations. *State of the Planet*, *2-oae2023*, 1–14. https://doi.org/10.5194/sp-2-oae2023-2-2023

Smith, S. V., & Key, G. S. (1975). Carbon dioxide and metabolism in marine environments. *Limnology and Oceanography*, *20*(3), 493–495. https://doi.org/10.4319/lo.1975.20.3.0493

Smith, S. V., & Kinsey, D. W. (1976). Calcium carbonate production, coral reef growth, and sea level change. *Science*, *194*(4268), 937–939. https://doi.org/10.1126/science.194.4268.937

Smith, S. V., & Mackenzie, F. T. (2016). The role of $CaCO_3$ reactions in the contemporary oceanic CO_2 cycle. *Aquatic Geochemistry*, *22*(2), 153–175. https://doi.org/10.1007/s10498-015-9282-y

Soetaert, K., Hofmann, A. F., Middelburg, J. J., Meysman, F. J. R., & Greenwood, J. (2007). The effect of biogeochemical processes on pH. *Marine Chemistry*, *105*(1–2), 30–51. https://doi.org/10.1016/j.marchem.2006.12.012

Subhas, A. V., Dong, S., Naviaux, J. D., Rollins, N. E., Ziveri, P., Gray, W., et al. (2022). Shallow calcium carbonate cycling in the North Pacific Ocean. *Global Biogeochemical Cycles*, *36*(5), e2022GB007388. https://doi.org/10.1029/2022GB007388

Suchet, P. A., Probst, J., & Ludwig, W. (2003). Worldwide distribution of continental rock lithology: Implications for the atmospheric/soil CO_2 uptake by continental weathering and alkalinity river transport to the oceans. *Global Biogeochemical Cycles*, *17*(2), 1038. https://doi.org/10.1029/2002GB001891

Sulpis, O., Jeansson, E., Dinauer, A., Lauvset, S. K., & Middelburg, J. J. (2021). Calcium carbonate patterns in the ocean. *Nature Geoscience*, *14*(6), 423–428. https://doi.org/10.1038/s41561-021-00743-y

Thomas, H., Schiettecatte, L.-S., Suykens, K., Koné, Y. J. M., Shadwick, E. H., Prowe, A. E. F., et al. (2009). Enhanced ocean carbon storage from anaerobic alkalinity generation in coastal sediments. *Biogeosciences*, *6*(2), 267–274. https://doi.org/10.5194/bg-6-267-2009

van de Velde, S. J., Vervoort, P., Smith, R. O., Law, C. S., & Currie, K. (2026). Anthropogenically stimulated carbonate dissolution in the global shelf seafloor is potentially an important and fast climate feedback. *AGU Advances*, *7*(1), e2025AV001865. https://doi.org/10.1029/2025AV001865

van Weering, T. C. E., Hall, I. R., de Stigter, H. C., McCave, I. N., & Thomsen, L. (1998). Recent sediments, sediment accumulation and carbon burial at Goban Spur, N.W. European Continental Margin (47–50°N). *Progress in Oceanography*, *42*(1–4), 5–35. https://doi.org/10.1016/S0079-6611(98)00026-3

Vecsei, A. (2004). A new estimate of global reefal carbonate production including the fore-reefs. *Global and Planetary Change*, *43*(1–2), 1–18. https://doi.org/10.1016/j.gloplacha.2003.12.002

Viechtbauer, W. (2010). Conducting meta-analyses in R with the metafor package. *Journal of Statistical Software*, *36*(3), 1–48. https://doi.org/10.18637/jss.v036.i03

Wallmann, K., Diesing, M., Scholz, F., Rehder, G., Dale, A. W., Fuhr, M., & Suess, E. (2022). Erosion of carbonate-bearing sedimentary rocks may close the alkalinity budget of the Baltic Sea and support atmospheric CO_2 uptake in coastal seas. *Frontiers in Marine Science*, *9*, 968069. https://doi.org/10.3389/fmars.2022.968069

Walter, L. M., & Burton, E. A. (1990). Dissolution of recent platform carbonate sediments in marine pore fluids. *American Journal of Science*, *290*(6), 601–643. https://doi.org/10.2475/ajs.290.6.601

Walter, L. M., & Morse, J. W. (1985). The dissolution kinetics of shallow marine carbonates in seawater: A laboratory study. *Geochimica et Cosmochimica Acta*, *49*(7), 1503–1513. https://doi.org/10.1016/0016-7037(85)90255-8

Watanabe, A., & Nakamura, T. (2019). Carbon dynamics in coral reefs. In *Blue carbon in shallow coastal ecosystems* (pp. 273–293). Springer. https://doi.org/10.1007/978-981-13-1295-3_10

Webb, J. E., & Theodor, J. (1968). Irrigation of submerged marine sands through wave action. *Nature*, *220*(5168), 682–683. https://doi.org/10.1038/220682a0

Wollast, R. (1994). The relative importance of biomineralization and dissolution of $CaCO_3$ in the global carbon cycle. In *Bulletin de l'Institut Océanographique, Monaco* (Vol. 13, pp. 13–35).

Yates, K. K., & Halley, R. B. (2003). Measuring coral reef community metabolism using new benthic chamber technology. *Coral Reefs*, *22*(3), 247–255. https://doi.org/10.1007/s00338-003-0314-5

Zeebe, R. E., & Wolf-Gladrow, D. (2001). *CO_2 in seawater: Equilibrium, kinetics, isotopes*. Gulf Professional Publishing.

Zhang, S., & Planavsky, N. J. (2020). Revisiting groundwater carbon fluxes to the ocean with implications for the carbon cycle. *Geology*, *48*(1), 67–71. https://doi.org/10.1130/G46408.1

References From the Supporting Information

Balzer, W., & Wefer, G. (1981). Dissolution of carbonate minerals in a subtropical shallow marine environment. *Marine Chemistry*, *10*(6), 545–558. https://doi.org/10.1016/0304-4203(81)90007-4

Barnes, D. J., & Devereux, M. J. (1984). Productivity and calcification on a coral reef: A survey using pH and oxygen electrode techniques. *Journal of Experimental Marine Biology and Ecology*, *79*(3), 213–231. https://doi.org/10.1016/0022-0981(84)90196-5

Berelson, W. M., McManus, J., Coale, K. H., Johnson, K. S., Kilgore, T., Burdige, D., & Pilskaln, C. (1996). Biogenic matter diagenesis on the sea floor: A comparison between two continental margin transects. *Journal of Marine Research*, *54*(4), 731–762. https://doi.org/10.1357/0022240963213673

Berelson, W. M., McManus, J., Coale, K., Johnson, K., Burdige, D., Kilgore, T., et al. (2003). A time series of benthic flux measurements from Monterey Bay, CA. *Continental Shelf Research*, *23*(5), 457–481. https://doi.org/10.1016/S0278-4343(03)00009-8

Berner, E. K., & Berner, R. A. (2012). *Global environment: Water, air, and geochemical cycles*. Princeton University Press.

Berner, R. A. (1982). Burial of organic carbon and pyrite sulfur in the modern ocean; its geochemical and environmental significance. *American Journal of Science*, *282*(4), 451–473. https://doi.org/10.2475/ajs.282.4.451

Boucher, G., Clavier, J., Hily, C., & Gattuso, J.-P. (1998). Contribution of soft-bottoms to the community metabolism (primary production and calcification) of a barrier reef flat (Moorea, French Polynesia). *Journal of Experimental Marine Biology and Ecology*, *225*(2), 269–283. https://doi.org/10.1016/S0022-0981(97)00227-X

Brenner, H., Braeckman, U., Le Guitton, M., & Meysman, F. J. R. (2016). The impact of sedimentary alkalinity release on the water column CO_2 system in the North Sea. *Biogeosciences*, *13*(3), 841–863. https://doi.org/10.5194/bg-13-841-2016

Conand, C., Chabanet, P., Cuet, P., & Letourneur, Y. (1997). The carbonate budget of a fringing reef in La Reunion Island (Indian Ocean): Sea urchin and fish bioerosion and net calcification. In *Proceedings of 8th International Coral Reef Symposium* (pp. 953–958). Retrieved from https://www.researchgate.net/publication/284047339

Cyronak, T., Santos, I. R., McMahon, A., & Eyre, B. D. (2013a). Carbon cycling hysteresis in permeable carbonate sands over a diel cycle: Implications for ocean acidification. *Limnology and Oceanography*, *58*(1), 131–143. https://doi.org/10.4319/lo.2013.58.1.0131

Galloway, J. N., Dentener, F. J., Capone, D. G., Boyer, E. W., Howarth, R. W., Seitzinger, S. P., et al. (2004). Nitrogen cycles: Past, present, and future. *Biogeochemistry*, *70*(2), 153–226. https://doi.org/10.1007/s10533-004-0370-0

Hedges, J. I., Baldock, J. A., Gélinas, Y., Lee, C., Peterson, M. L., & Wakeham, S. G. (2002). The biochemical and elemental compositions of marine plankton: A NMR perspective. *Marine Chemistry*, *78*(1), 47–63. https://doi.org/10.1016/S0304-4203(02)00009-9

Hu, X., & Cai, W. J. (2011). An assessment of ocean margin anaerobic processes on oceanic alkalinity budget. *Global Biogeochemical Cycles*, *25*(3), GB3003. https://doi.org/10.1029/2010GB003859

Isson, T. T., & Planavsky, N. J. (2018). Reverse weathering as a long-term stabilizer of marine pH and planetary climate. *Nature*, *560*(7719), 471–475. https://doi.org/10.1038/s41586-018-0408-4

Leclercq, N., Gattuso, J.-P., & Jaubert, J. (2002). Primary production, respiration, and calcification of a coral reef mesocosm under increased CO_2 partial pressure. *Limnology and Oceanography*, *47*(2), 558–564. https://doi.org/10.4319/lo.2002.47.2.0558

Mucci, A., Sundby, B., Gehlen, M., Arakaki, T., Zhong, S., & Silverberg, N. (2000). The fate of carbon in continental shelf sediments of eastern Canada: A case study. *Deep-Sea Research II*, *47*(3–4), 733–760. https://doi.org/10.1016/S0967-0645(99)00124-1

Rude, P. D., & Aller, R. C. (1991). Fluorine mobility during early diagenesis of carbonate sediment: An indicator of mineral transformations. *Geochimica et Cosmochimica Acta*, *55*(9), 2491–2509. https://doi.org/10.1016/0016-7037(91)90368-F

Silverberg, N., Sundby, B., Mucci, A., Zhong, S., Arakaki, T., Hall, P., et al. (2000). Remineralization of organic carbon in eastern Canadian continental margin sediments. *Deep-Sea Research II*, *47*(3–4), 699–731. https://doi.org/10.1016/S0967-0645(99)00123-X

Silverman, J., Lazar, B., & Erez, J. (2007). Effect of aragonite saturation, temperature, and nutrients on the community calcification rate of a coral reef. *Journal of Geophysical Research*, *112*(C5), C05004. https://doi.org/10.1029/2006JC003770

Slomp, C. P., & Van Cappellen, P. (2004). Nutrient inputs to the coastal ocean through submarine groundwater discharge: Controls and potential impact. *Journal of Hydrology*, *295*(1–4), 64–86. https://doi.org/10.1016/j.jhydrol.2004.02.018

Suykens, K., Schmidt, S., Delille, B., Harlay, J., Chou, L., De Bodt, C., et al. (2011). Benthic remineralization in the northwest European continental margin (northern Bay of Biscay). *Continental Shelf Research*, *31*(6), 644–658. https://doi.org/10.1016/j.csr.2010.12.017

Wallmann, K., Aloisi, G., Haeckel, M., Tishchenko, P., Pavlova, G., Greinert, J., et al. (2008). Silicate weathering in anoxic marine sediments. *Geochimica et Cosmochimica Acta*, *72*(12), 2895–2918. https://doi.org/10.1016/j.gca.2008.03.026

Wallmann, K., Pinero, E., Burwicz, E., Haeckel, M., Hensen, C., Dale, A., & Ruepke, L. (2012). The global inventory of methane hydrate in marine sediments: A theoretical approach. *Energies*, *5*(7), 2449–2498. https://doi.org/10.3390/en5072449

Yates, K. K., & Halley, R. B. (2006a). CO_3^{2-} concentration and pCO_2 thresholds for calcification and dissolution on the Molokai reef flat, Hawaii. *Biogeosciences*, *3*, 357–369. https://doi.org/10.5194/bg-3-357-2006

Yates, K. K., & Halley, R. B. (2006b). Diurnal variation in rates of calcification and carbonate sediment dissolution in Florida Bay. *Estuaries and Coasts*, *29*(1), 24–39. https://doi.org/10.1007/BF02784696

Zhou, Y., Sawyer, A. H., David, C. H., & Famiglietti, J. S. (2019). Fresh submarine groundwater discharge to the near-global coast. *Geophysical Research Letters*, *46*(11), 5855–5863. https://doi.org/10.1029/2019GL082749